The Journal of Immunology

CCR2 Identifies a Stable Population of Human Effector Memory CD4 $^{+}$ T Cells Equipped for Rapid Recall Response

Hongwei H. Zhang, Kaimei Song, Ronald L. Rabin, Brenna J. Hill, Stephen P. Perfetto, Mario Roederer, Daniel C. Douek, Richard M. Siegel and Joshua M. Farber

J Immunol 2010; 185:6646-6663; Prepublished online 27 October 2010;
doi: 10.4049/jimmunol.0904156
http://www.jimmunol.org/content/185/11/6646

The Journal of Immunology is published twice each month by
The American Association of Immunologists, Inc.,
1451 Rockville Pike, Suite 650, Rockville, MD 20852

Print ISSN: 0022-1767 Online ISSN: 1550-6606.

CCR2 Identifies a Stable Population of Human Effector Memory CD4$^+$ T Cells Equipped for Rapid Recall Response

Hongwei H. Zhang,*[,1] Kaimei Song,*[,1,2] Ronald L. Rabin,[†] Brenna J. Hill,[‡] Stephen P. Perfetto,[§] Mario Roederer,[§] Daniel C. Douek,[‡] Richard M. Siegel,[¶] and Joshua M. Farber*

Because T cells act primarily through short-distance interactions, homing receptors can identify colocalizing cells that serve common functions. Expression patterns for multiple chemokine receptors on CD4$^+$ T cells from human blood suggested a hierarchy of receptors that are induced and accumulate during effector/memory cell differentiation. We characterized CD4$^+$CD45RO$^+$ T cells based on expression of two of these receptors, CCR5 and CCR2, the principal subsets being CCR5$^-$CCR2$^-$ (~70%), CCR5$^+$CCR2$^-$ (~25%), and CCR5$^+$CCR2$^+$ (~5%). Relationships among expression of CCR5 and CCR2 and CD62L, and the subsets' proliferation histories, suggested a pathway of progressive effector/memory differentiation from the CCR5$^-$CCR2$^-$ to CCR5$^+$CCR2$^-$ to CCR5$^+$CCR2$^+$ cells. Sensitivity and rapidity of TCR-mediated activation, TCR signaling, and effector cytokine production by the subsets were consistent with such a pathway. The subsets also showed increasing responsiveness to IL-7, and the CCR5$^+$CCR2$^+$ cells were CD127^{bright} and invariably showed the greatest response to tetanus toxoid. CCR5$^+$CCR2$^+$ cells also expressed the largest repertoire of chemokine receptors and migrated to the greatest number of chemokines. By contrast, the CCR5$^+$CCR2$^-$ cells had the greatest percentages of regulatory T cells, activated/cycling cells, and CMV-reactive cells, and were most susceptible to apoptosis. Our results indicate that increasing memory cell differentiation can be uncoupled from susceptibility to death, and is associated with an increase in chemokine responsiveness, suggesting that vaccination (or infection) can produce a stable population of effector-capable memory cells that are highly enriched in the CCR5$^+$CCR2$^+$ subset and ideally equipped for rapid recall responses in tissue. ***The Journal of Immunology*****, 2010, 185: 6646–6663.**

The study of immunological memory has potential implications for the development of novel vaccines (1) and for immune reconstitution in individuals made immunodeficient by disease or as a result of therapeutic interventions (2). Understanding how immunological memory functions requires characterizing the development and organization of functional subsets of effector/memory cells. Both CD8 and CD4 cells differentiate through a multistep process to produce heterogeneous populations of effector and memory cells (3–5).

CD4$^+$ effector/memory T cells can be divided into subsets based on their patterns of cytokine production (4, 6, 7) and/or regulatory activities (6, 8) and/or surface markers related to T cell activation and survival (9, 10). In addition to the changes in these parameters, differentiation from naive to effector/memory T cells is accompanied by significant changes in T cell trafficking within lymphoid compartments (11) and in the cells' acquisition of access to sites in nonlymphoid tissues (12). These changes are the result of the selective loss and/or induction of adhesion molecules and chemoattractant receptors (13). The associations among these surface molecules, trafficking behavior, and other aspects of the cells' phenotypes have been used to define novel T cell subsets that in turn have enhanced our understanding of the pathways for generating effector/memory cells.

CD4$^+$ T cells function at organ and tissue sites through cell–cell or short-distance interactions. Chemokine receptors, by identifying cells that are co-recruited, should therefore define subsets of cells that act together in an immune response, and whose analysis as a subset is biologically relevant. For example, the study of CCR7, which, together with CD62L, is required for mouse T cells to enter noninflamed lymph nodes from the blood (14, 15), has revealed important connections between migratory properties and broader functional features. CCR7 and CD62L have been used extensively to separate memory cells into "central," CCR7$^+$/CD62L$^+$ (T_{CM}) and "effector," CCR7$^-$/CD62L$^-$ (T_{EM}) subsets. According to the T_{CM}/T_{EM} model as proposed by Sallusto and colleagues (16–18), T_{CM} cells circulate among lymphoid organs and do not show efficient effector functions. T_{EM} cells are excluded from lymphoid organs, are capable of entering peripheral tissues, and can demonstrate immediate effector functions such as, for CD4$^+$ T cells, the production of effector cytokines. One component of the model is the ordering of T cells within the memory population along a linear pathway of differentiation, with T_{CM} serving as a pool of precursors for the production of T_{EM}.

*Inflammation Biology Section, Laboratory of Molecular Immunology, [‡]Human Immunology Section, and [§]ImmunoTechnology Section, Vaccine Research Center, National Institute of Allergy and Infectious Diseases; [¶]Autoimmunity Branch, National Institute of Arthritis and Musculoskeletal and Skin Diseases, National Institutes of Health; and [†]Center for Biologics Evaluation and Research, U.S. Food and Drug Administration, Bethesda, MD 20892

[1]H.H.Z. and K.S. contributed equally to this work.

[2]Current address: ImmunoTechnology Section, Vaccine Research Center, National Institute of Allergy and Infectious Diseases, National Institutes of Health, Bethesda, MD.

Received for publication December 28, 2009. Accepted for publication September 19, 2010.

This work was supported by the Intramural Research Program of the National Institute of Allergy and Infectious Diseases, National Institutes of Health.

Address correspondence and reprint requests to Dr. Joshua M. Farber, Building 10, Room 11N-112, 10 Center Drive, National Institutes of Health, Bethesda, MD 20892. E-mail address: jfarber@niaid.nih.gov

The online version of this article contains supplemental material.

Abbreviations used in this paper: DDAO, dodecyldimethylamine oxide; MFI, mean fluorescent intensity; PI, propidium iodide; RT, room temperature; TBST, Tris-buffered saline with Tween 20; T_{CM}, central memory T cell; T_{EM}, effector memory T cell; TetTx, tetanus toxoid; TREC, TCR-rearrangement excision circles; Treg, regulatory T cell; TSST, toxic shock syndrome toxin.

www.jimmunol.org/cgi/doi/10.4049/jimmunol.0904156

Studies of $CD4^+$ T cells in mice have supported a number of aspects of the T_{CM}/T_{EM} model, and have shown, for example, that memory cells with effector function migrate to and survive in peripheral tissues (19–21), and that cells in peripheral tissue have enhanced effector function and are $CD62L^-$ (22). More complex and controversial are the pathways for generating and maintaining T_{CM} and T_{EM}, and the specific contributions of these subsets to long-term protection (23–31). T_{EM} have been described as having higher rates of cell division (32) and cell death (33–35), leading to the proposition that the T_{EM} are a short-lived population.

By comparing expression of a number of chemokine receptors with CD62L on $CD4^+$ T cells from blood, we found that CCR5 and CCR2 were opposed to CCR7 in being most skewed toward $CD62L^-$ cells. CCR5 is a receptor for CCL3-5 as well as CCL's 8, 13, and 14. CCR5 shows some preferential expression on Th1 versus Th2 cells, and serves as the primary coreceptor, together with CD4, for HIV-1 (reviewed in Ref. 36). CCR2 is closely related to CCR5 (76% sequence identity), and the genes for CCR2 and CCR5 are adjacent on human chromosome 3p21. CCR2 is a receptor for CCL2, 7, 8, and 13, and is a major receptor for monocyte recruitment (reviewed in Ref. 37). Like CCR5, CCR2 has been reported to show some preferential expression on Th1 cells (38) and can function, although for a very limited number of viral strains, as a coreceptor for HIV-1 (39).

To understand the functions of the $CD4^+$ T cells expressing CCR5 and CCR2 within the effector/memory population, and the possible roles of CCR5 and CCR2 on these cells, we analyzed effector/memory cells divided into the following principal subsets defined by CCR5 and CCR2: $CCR5^-CCR2^-$, $CCR5^+CCR2^-$, and $CCR5^+CCR2^+$. Our data suggest a pathway of progressive differentiation from $CCR5^-CCR2^-$ to $CCR5^+CCR2^-$ to $CCR5^+CCR2^+$ cells and have implications for understanding the origins, maintenance, and functions of memory subsets. One conclusion suggested by our findings is that memory cells within the $CCR5^+CCR2^+$ subset have characteristics of a stable population that can migrate to any of multiple inflammatory chemokines and that can respond rapidly to submaximal stimulation to secrete effector cytokines. Together, these features suggest that the $CCR5^+CCR2^+$ subset contains long-term memory cells that are well equipped for mounting rapid responses to secondary challenges.

Materials and Methods

Cells

Whole blood and elutriated lymphocytes were obtained from healthy donors by the Department of Transfusion Medicine, Clinical Center, National Institutes of Health, Bethesda, MD, under a protocol approved by the Institutional Review Board.

Abs and flow cytometry

All Abs were against human Ags. Anti–CCR2-biotin, anti–CCR2-allophycocyanin, anti–CCR4-allophycocyanin, anti–CCR7-FITC, anti–CXCR3-FITC, and anti–CXCR5-FITC were purchased from R&D Systems (Minneapolis, MN). Anti–CD4-cascade blue, anti–CD4-allophycocyanin-Cy7, anti–CD4-FITC, anti–CD62L-FITC, anti–CCR5-PE-Cy5, anti–CCR5-FITC, anti–CD45RO-PE-Cy5, anti–CD45RA-PE-Cy5, anti–CD45RO-PE-Cy7, anti–CCR6-PE, anti–CD3-biotin, anti–CD25-allophycocyanin, anti–CD25-allophycocyanin-Cy7, anti–CD122-PE, anti–CD26-FITC, anti–CD127-PE, anti–CD127-allophycocyanin, anti–CD132-PE, anti–HLA-DR-allophycocyanin, anti–HLA-DR-FITC, anti–IL-2-FITC, anti–IFN-γ-FITC, anti–IFN-γ-PE-Cy7, anti–TNF-α-allophycocyanin, anti–TNF-α-Alexa 700, anti–Ki67-PE, anti–Ki67-FITC, and anti–BCL-2-FITC were purchased from BD Biosciences (San Jose, CA). Qdot655-conjugated streptavidin was from Invitrogen (Carlsbad, CA). Anti-CD3 was obtained from BD Pharmingen (San Diego, CA) and conjugated to Qdot605 according to the manufacturer's protocol (Invitrogen, Carlsbad, CA). Anti–FOXP3-Alexa Fluor 700 was from eBioscience (San Diego, CA). For phenotypic analysis of leukocyte subsets, cells were stained in whole blood, in preparations of PBMCs isolated from blood using Ficoll/Hypaque (Amersham Biosciences, Piscataway, NJ), or in preparations of $CD4^+$ T cells purified from elutriated lymphocytes using RosetteSep (StemCell Technologies, Vancouver, British Columbia, Canada). For staining cells in whole blood, we used 100 μl blood, and for staining other samples, 100 μl 1×10^7 cells/ml in HBSS (Mediatech, Manassas, VA) plus 2% FBS (HBSS/FBS, with FBS obtained from Gemini Bio-Products, Woodland, CA). Cells were incubated with 1 μg fluorescent-conjugated primary Abs for 15 min at room temperature (RT), and washed with HBSS/FBS. For whole blood samples, red cells were then removed using Pharm Lyse (BD Biosciences) according to the manufacturer's protocol. For cells stained with anti–CCR2-biotin, the cells were incubated with PE- or Qdot655-conjugated streptavidin for an additional 15 min at RT. Cells were fixed in 1% paraformaldehyde. Staining data were collected on a FACSCalibur or LSR II cytometer (BD Biosciences). To set gates for defining positive and negative cells in multicolor staining, samples were stained with a mixture of all Abs save one. Flow cytometry data were analyzed using FlowJo (Tree Star, Ashland, OR).

Measuring TCR-rearrangement excision circles

Approximately 1.5×10^8 $CD4^+$ T cells were isolated from elutriated lymphocytes to > 95% purity using RosetteSep (StemCell Technologies) and incubated with anti–CCR2-biotin and anti–CCR5-PE-Cy5 in HBSS plus 4% FBS for 15 min at RT. Following washing, the cells were stained with streptavidin-PE, anti–CD4-FITC, and anti–CD45RO-allophycocyanin for an additional 15 min at RT. The cells were washed and resuspended in HBSS plus 4% FBS, and cell subsets were isolated to nearly 100% purity using an Aria cytometer (BD Biosciences). The sorted cells were analyzed for TCR-rearrangement excision circles (TREC), using real-time quantitative PCR with normalization based on copies of the albumin gene, as described (40).

Measuring CD3-mediated calcium signals

$CD4^+$ T cells were purified from elutriated lymphocytes using RosetteSep (StemCell Technologies), and the $CD45RA^-$ effector/memory cells were purified using magnetic beads according to the manufacturer's protocol (Miltenyi Biotec, Auburn, CA). Aliquots of total $CD4^+$ or $CD45RA^-$ cells were loaded in 5 μM indo-1 AM ester (Molecular Probes, Eugene, OR) for 45 min at 32°C. To analyze naive cells, the total $CD4^+$ T cells were then incubated with anti–CD4-allophycocyanin-Cy7, anti–CD45RO-PE-Cy5, and 20 μg/ml biotin-conjugated anti-CD3 for 20 min at RT. To analyze effector/memory cells, the $CD45RA^-$ cells were then incubated with anti–CD4-allophycocyanin-Cy7, anti–CD45RO-PE-Cy5 or anti–CD45RA-PE-Cy5, anti–CCR2-allophycocyanin, anti–CCR5-FITC, and 20 μg/ml biotin-conjugated anti-CD3. Cells were warmed to 37°C, and the ratio of 405/20 nm: 525/20 nm emissions was measured on an LSR II cytometer before and after CD3 cross-linking, using 10 μg/ml avidin (Sigma-Aldrich, St. Louis, MO). The data were analyzed using FlowJo (Tree Star).

Detecting CD154

$CD4^+$ T cells were purified from elutriated lymphocytes using RosetteSep (StemCell Technologies) and incubated first with anti–CCR2-biotin and anti–CCR5-PE-Cy5 in HBSS plus 4% FBS for 15 min at RT. After washing, cells were incubated with streptavidin-PE, anti–CD45RO-allophycocyanin, and a mixture of anti–CD8-FITC, anti–CD14-FITC, anti–CD16-FITC, anti–CD19-FITC, and anti–CD56-FITC for another 15 min at RT. Cells were washed again and resuspended in HBSS plus 4% FBS to sort for subsets to nearly 100% purity on an Aria cytometer (BD Biosciences), using FITC as a "dump" channel. For detecting CD154, for CFSE proliferation assays, and for analysis of cytokine production by intracellular staining (see below), cells were sorted using either a "dump" channel or anti-CD4, and no differences were found in the subsets' responses (data not shown). For analyzing CD154 induction in $CCR7^+/CCR7^-$ cells, staining was done with anti–CD4-allophycocyanin-Cy7, anti–CD45RO-FITC, anti–CCR5-PE-Cy5, anti–CCR2-biotin with streptavidin-PE, and anti–CCR7-PE-Cy7 before sorting. Purified subsets of $CD4^+$ T cells were resuspended at 2×10^5 cells/200 μl in RPMI 1640 media supplemented with 10% FBS, 2 mM L-glutamine, 100 U/ml penicillin, and 100 μg/ml streptomycin (all from Invitrogen except FBS) and cultured in a 96-well flat-bottom plate (Corning, Corning, NY). Some cells were activated using 10 μg/ml plate-bound anti-CD3 (Clone OKT3, obtained from Ortho Biotech, Bridgewater, NJ) plus 1 μg/ml soluble anti-CD28 (clone CK248, kindly provided by Calman Prussin, Laboratory of Allergic Diseases, National Institute of Allergy and Infectious Diseases, National Institutes of Health, Bethesda, MD). For superantigen stimulation, the purified subsets of $CD4^+$ T cells were cultured together with 1×10^6 CFSE-labeled PBMCs/well in the presence of 1 μg/ml toxic shock syndrome toxin 1 (TSST-1; Sigma Aldrich). Anti–CD154-allophycocyanin and 2 μM monensin (BD Biosciences) were included in

both cultures during the stimulation. Cells were harvested after 6 h and washed with HBSS plus 2% FBS before analysis on an LSR II cytometer.

Measuring proliferation and cytokine production

For assays using CFSE dilution, subsets of $CD4^+$ T cells were purified by cell sorting as for measuring TREC (see above), and cells were loaded with 8 μM CFSE (Invitrogen) for 10 min at RT and then resuspended in RPMI 1640 media supplemented with 10% FBS, 2 mM L-glutamine, 1 mM sodium pyruvate, 0.1 mM nonessential amino acids, 55 μM 2-ME, 100 U/ml penicillin, and 100 μg/ml streptomycin (complete medium). Some cells were diluted to 2×10^5 cells/200 μl and activated using 10 μg/ml plate-bound anti-CD3 plus 1 μg/ml soluble anti-CD28. For activation using beads, cells were first incubated with magnetic beads conjugated with anti-CD3 and anti-CD28 (gift from Daniel Fowler, Experimental Transplantation and Immunology Branch, Center for Cancer Research, National Cancer Institute, National Institutes of Health, Bethesda, MD), at a ratio of 3 beads/1 cell, in 30 μl for 30 min at 37°C with rotation and then resuspended at 2×10^5 cells/200 μl for culturing in a 96-well plate. For analyzing responses to IL-7 and/or IL-15, cells were cultured with 25 ng/ml each cytokine (both from R&D Systems). Cells were harvested after 3 or 7 d. CFSE profiles of viable cells were analyzed on an LSR II cytometer. Dead cells were excluded from the analysis, using propidium iodide (PI; Caltag Laboratories, Burlingame, CA). For assays using incorporation of [^{3}H]thymidine, subsets of $CD4^+$ T cells were purified by cell sorting, as for measuring TREC (see above), or after staining with anti–CD4-FITC, anti–CD45RO-PE-Cy7, anti–CCR2-biotin with streptavidin-PE, anti–CCR5-PE-Cy5, anti–CD25-allophycocyanin-Cy7, and anti–CD127-allophycocyanin. Purified cells were diluted in complete medium to 2×10^5 cells/200 μl into a 96-well plate and activated by various concentrations of plate-bound anti-CD3 plus 1 μg/ml soluble anti-CD28 for 2 d, followed by pulsing with 1 μCi [^{3}H]thymidine (PerkinElmer, Wellesley, MA) for another 16 h at 37°C. The cells were harvested and washed using a Harvester 96 (Tomtec, Hamden, CT). Radioactivity was measured in a 1450 LSC & Luminescence Counter (PerkinElmer). For measuring cytokine production, sorted cells were incubated in complete medium for 16 h at 37°C before supernatants were harvested and analyzed using ELISA by SearchLight Technology, Pierce Biotechnology (Thermo Fisher Scientific, Rockford, IL).

RNA isolation and real-time fluorogenic RT-PCR

Subsets of $CD4^+$ T cells were purified by cell sorting as for measuring TREC (see above), and 1×10^6 cells were stimulated with 20 ng/ml PMA plus 1 μM ionomycin in a total volume of 1 ml in 24-well plates for 3 h at 37°C. Total cellular RNA was isolated using the TRIzol reagent (Invitrogen). Real-time RT-PCR was performed with 50 ng RNA as a template, using the SuperScript One-Step RT-PCR Kit (Invitrogen). Primer and probe sets (FAM/MGB-labeled) were purchased from Applied Biosystems (Foster City, CA). Results were normalized based on the values for *GAPDH*, detected using TaqMan *GAPDH* control reagents (Applied Biosystems). Real-time PCR analysis was performed on samples in duplicate using an ABI 7700 Sequence Detection System (Applied Biosystems). For cells from each donor, relative levels of expression, based on values for $2^{-\Delta CT}$, are shown as percentages of the subset with the highest value.

Intracellular staining for cytokines

Subsets of $CD4^+$ T cells were purified by cell sorting, as for measuring TREC; as for measuring proliferation to exclude $CD25^+$ and $CD127^-$ cells; or as for detecting CD154 to divide subsets further based on expression of CCR7 (see above). A total of 1×10^6 cells were stimulated with 20 ng/ml PMA plus 1 μM ionomycin in the presence of 2 μM monensin or Leukocyte Activation Cocktail with GolgiPlus (BD Biosciences) in a total volume of 1 ml in 24-well plates for 4 h at 37°C. Cells were then fixed and permeabilized using a Cytofix/CytoPerm Plus Kit (BD Biosciences) before staining with anti–IL-2-FITC, anti–IFN-γ-PE-Cy7, and anti–TNF-α-allophycocyanin or with anti–IFN-γ-FITC and anti–TNF-α-Alexa700. Staining data were collected on an LSR II cytometer (BD Biosciences) and analyzed using FlowJo software (Tree Star).

Ag-specific responses

Subsets of $CD4^+$ T cells were purified by cell sorting as for measuring TREC, or as for measuring proliferation to exclude only $CD25^+$ or $CD25^+$ plus $CD127^-$ cells (see above). Purified cells were loaded with 8 μM CFSE (Invitrogen) for 10 min at RT, and then resuspended at 1×10^5 cells/ml in complete medium. PBMCs from the same donor were labeled with 2 μM CellTrace Far Red DDAO-SE (Molecular Probes) for 10 min at RT, irradiated with 2000 rad, and then resuspended at 5×10^5 cells/ml in complete medium. Equal volumes of sorted cells and PBMCs were mixed and cultured in a 24-well plate for 7 d at 37°C in the presence or absence of 10 μg/ml tetanus toxoid (University of Massachusetts or Statens Serum Institute, Copenhagen, Denmark) or extracts from control or virus-infected cells (EastCoast Bio, North Berwick, ME). HSV-1 was grown in VERO cells, and extracts were used at a dilution of 1:600; EBV was grown in human B cells, and extracts were used at a dilution of 1:500; and CMV was grown in normal human dermal fibroblasts, and extracts were used at

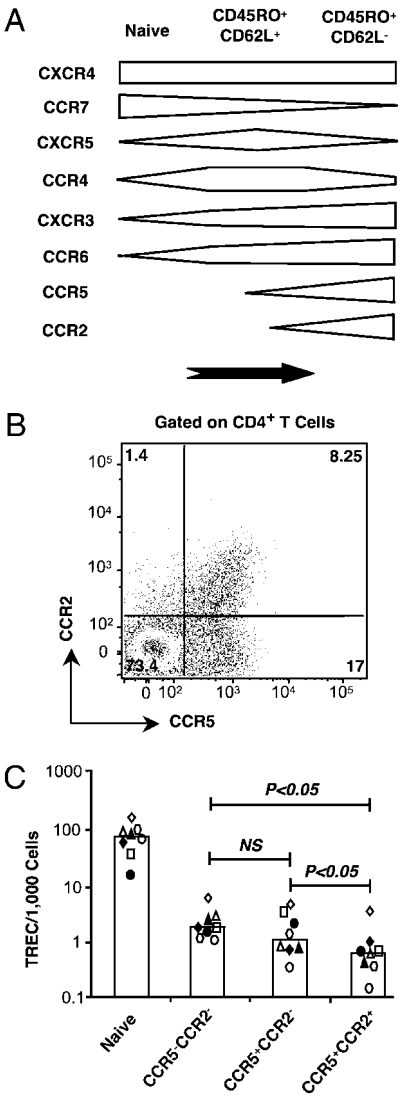

FIGURE 1. Patterns suggest late and sequential induction of CCR5 and CCR2 on effector/memory $CD4^+$ T cells. *A*, Cells were stained in whole blood or from PBMCs, and the percentages of cells staining for each chemokine receptor were analyzed in naive ($CD4^+CD45RO^-CD62L^+$), $CD4^+CD45RO^+CD62L^+$, and $CD4^+CD45RO^+CD62L^-$ subsets. The relative numbers of receptor$^+$ cells within the three subsets are represented graphically for each receptor, based on the results from more than 20 donors. The horizontal arrow indicates the direction of increasing proliferation and differentiation. *B*, Purified $CD4^+$ T cells were stained with anti–CD4-FITC, anti–CCR5-PE-Cy5, and anti–CCR2-biotin plus streptavidin-PE. In these and all other flow cytometry data, analysis included an initial gating based on forward and side scatter. Only $CD4^+$ cells are shown. Quadrant boundaries were set based on samples stained with all Abs except one. Results are representative of data from more than 30 donors. *C*, Purified $CD4^+$ T cells from each of eight donors were sorted into naive ($CD45RO^-$) and the three $CD45RO^+$ subsets based on CCR5 and CCR2 for measuring TREC. TREC values are expressed per 1000 cells based on albumin gene copy number. Each donor is represented by a unique symbol. Open bars show medians. *p* values were determined using the Wilcoxon matched-pairs signed-rank test. In addition to the comparisons marked by the horizontal lines, values for all the $CD45RO^+$ subsets were significantly lower than values for the naive ($CD45RO^-$) cells.

a dilution of 1:300. Dilutions were based on titrations that established optimal proliferation responses while minimizing toxicity (data not shown). Cells were then harvested and stained with anti–CD3-allophycocyanin-Cy7, and anti–CD4-PE. PI was added, CFSE profiles of $CD3^+CD4^+$ PI^-DDAO^- cells were assessed, and cells were counted using AccuCount Fluorescent Particles (Spherotech, Libertyville, IL) on an LSR II cytometer.

Inducing and measuring cell death

Subsets of $CD4^+$ T cells were purified by cell sorting as for measuring TREC, or as for measuring proliferation to exclude only $CD25^+$ or $CD25^+$ plus $CD127^-$ cells (see above). Purified cells were resuspended at 2×10^5 cells/200 μl in complete medium and stimulated with either 10 μg/ml plate-bound anti-CD3 plus 1 μg/ml soluble anti-CD28 or 2 μg/ml soluble anti-Fas (Clone APO-1-3; Axxora, San Diego, CA) plus 1 μg/ml soluble anti-mouse IgG_3 (BD Biosciences) for 16 h at 37°C. Live and dead cells were distinguished according to their scatter profiles, and in some cases after staining with annexin V and PI, and counted using AccuCount Fluorescent Particles on an LSR II cytometer. Specific cell death was calculated from the following formula:

$$[1 - (\%\ \text{live cells treated}/\%\ \text{live cells untreated})] \times 100\%.$$

Western blotting

Subsets of $CD4^+$ T cells were purified by cell sorting as for measuring TREC (see above) and lysed on ice for 1 h in chilled lysis buffer (50 mM Tris HCl, pH 8.0; 150 mM NaCl; 1 mM EDTA; and 2% Triton X-100) containing 1:200 protease inhibitor mixture (Sigma-Aldrich). Cellular lysates were centrifuged at 12,000 × *g* for 10 min at 4°C, and supernatants were collected after centrifugation. Protein content was quantified using the Micro BCA Protein assay (Pierce) according to the manufacturer's guidelines with BSA as a standard. Samples were prepared for SDS-PAGE by boiling at 100°C with 2× Laemmli sample buffer (Bio-Rad, Hercules, CA) plus 8 M urea. A total of 10 μg cellular proteins were separated by SDS-PAGE in 4–15% acrylamide gradient gels (Bio-Rad) at 150 V. After electrophoresis, protein was transferred to an Immun-Blot polyvinylidene difluoride membrane (Bio-Rad Laboratories) over 1 h, using a Mini Trans-Blot Cell (Bio-Rad). Following transfer, the membrane was washed in Tris-buffered saline with Tween 20 (TBST) and blocked for 1 h in 5% nonfat dried skimmed milk powder in TBST. The membrane was then incubated for 2 h at RT with 1:500 dilution of mouse anti-human BCL-2 or mouse anti-human cFLIP (both from Axxora) in 5% skimmed milk TBST. Following incubation with primary Ab, the membrane was washed with TBST and incubated at RT with 1:1000 dilution of HRP-conjugated horse anti-mouse Ab (Cell Signaling Technology, Beverly, MA) in 5% skimmed milk TBST for 1 h, and then washed with TBST. Protein bands were visualized using SuperSignal West Pico Chemiluminescent Substrate (Pierce). Quantification of bands was done using Adobe Photoshop (San Jose, CA) and the ImageJ program (National Institutes of Health) as described on the following Web site: www.lukemiller.org/journal/2007/08/quantifying-Western-blots-without.html

Chemotaxis

Subsets of $CD4^+$ T cells were purified by cell sorting as for measuring TREC (see above) and resuspended at 1×10^7 cells/ml in RPMI 1640 supplemented with 0.5% BSA and 25 mM HEPES (chemotaxis medium). A total of 100 μl cells were added to each insert of the Transwell apparatus with 6.5-mm-diameter membranes containing 3.0-μm pores (Corning). The cells were preincubated for 30 min at 37°C, and the inserts were then transferred into wells with chemotaxis medium containing either chemokines (all from PeproTech, Rocky Hill, NJ) or macrophage-conditioned medium (diluted with the chemotaxis medium). Cells in the lower wells were harvested after 3 h at 37°C, and the migrated cells were counted using AccuCount Fluorescent Particles (Spherotech) on an LSR II cytometer.

Culturing macrophages

Monocytes were purified from elutriated mononuclear cells, using magnetic beads (Monocyte Isolation Kit II; Miltenyi Biotec), and cultured for 4 d in IMDM containing 10% human serum type AB (Sigma-Aldrich), 50 ng/ml recombinant human GM-CSF (R&D Systems), 100 μg/ml gentamicin sulfate, and 1 mM sodium pyruvate. The cells were then stimulated with 100 ng/ml LPS (*Salmonella abortus*; Sigma-Aldrich) for 2 d before the medium was harvested.

Statistics

Statistical comparisons used the Wilcoxon matched-pairs signed-rank test, ANOVA, or a two-tailed Student *t* test, as noted in the figure legends.

Results

CCR5 and CCR2 show a pattern suggesting late and sequential induction on $CD4^+$ T cells during naive → T_{CM} → T_{EM} differentiation

We stained subsets of $CD4^+$ T cells, as defined by CD45RO and CD62L, from the blood of healthy adults for the expression of 13 chemokine receptors, and found that 9 receptors were expressed on sufficient numbers of cells for analysis (data not shown). The $CD45RO^-CD62L^+$ phenotype has been used to identify naive cells (41, 42), and among the $CD45RO^+$ (effector/memory) cells, as noted above, CD62L expression, along with CCR7, has been used to identify cells in the T_{CM} versus the T_{EM} memory subsets (16, 17, 29). In analyzing $CD4^+$ T cells from more than 20 donors, general

Table I. *Protein staining for naive and effector/memory $CD4^+$ T cells*

	Naive ($CD45RO^-$)	Effector/Memory ($CD45RO^+$)		
		$CCR5^-CCR2^-$	$CCR5^+CCR2^-$	$CCR5^+CCR2^+$
CD62L	98.3 ± 0.4	82.3 ± 2.1***	65.6 ± 3.5***	49.2 ± 3.5**
CCR7	98.9 ± 0.3	87.7 ± 1.8***	45.8 ± 2.9***	43.9 ± 3.5
CD26	52.2 ± 4.5[a]	43.1 ± 2.1	49.7 ± 3.1[b]	73.0 ± 3.6***
CD27	98.1 ± 0.6	93.7 ± 0.7***	74.2 ± 3.4***	77.3 ± 1.8
CD28	96.6 ± 0.6	98.0 ± 0.6	93.8 ± 2.6	99.0 ± 0.2
CD122[c]	48.0 ± 2.3[a]	62.9 ± 2.4***	73.5 ± 3.0*	78.9 ± 2.5
CD127	59.4 ± 2.3[a]	72.9 ± 1.9***	52.4 ± 2.7***	68.8 ± 3.0***
CD132[c]	72.6 ± 3.1[a]	81.2 ± 2.8	86.2 ± 2.1	90.2 ± 1.7
CD25	3.2 ± 0.9	5.1 ± 0.5	19.9 ± 1.9***	8.8 ± 1.2***
FOXP3	0.2 ± 0	1.7 ± 0.2***	9.7 ± 1.0***	3.6 ± 0.4***
HLA-DR	0.9 ± 0.2	8.2 ± 0.9***	36.8 ± 1.9***	16.3 ± 1.8***
Ki67	0.5 ± 0	2.9 ± 0.3***	8.8 ± 0.5***	3.7 ± 0.3***
CXCR4	95.3 ± 1.2	77.2 ± 2.1***	50.7 ± 1.6***	59.4 ± 1.7***
CXCR5	3.8 ± 0.6	39.4 ± 2.7***	9.7 ± 1.6***	4.8 ± 1.4*

Mean percentage positive-staining cells ± SE from ≥10 donors.

[a]Naive cells were a homogenous population that straddled the channel separating positive from negative staining.

[b]Number of $CD26^+$ cells was significantly greater in the $CCR5^+CCR2^-$ subset than in the $CCR5^-CCR2^-$ subset by the Wilcoxon matched-pairs signed-rank test applied to data from multiple donors.

[c]Wilcoxon matched-pairs signed-rank test showed differences in expression among subsets (see Fig. 4 and text).

*$p < 0.05$; **$p < 0.01$; *** $p < 0.001$, using a two-tailed Student *t* test, compared with the percent positive cells for the subset to the immediate left.

patterns of chemokine receptor expression emerged, as diagrammed in Fig. 1*A*. As opposed to CCR7, which was enriched in the naive and $CD45RO^+CD62L^+$ cells and expressed at lower levels in the $CD45RO^+CD62L^-$ cells, CCR5 and CCR2 were relatively enriched in cells that had lost CD62L. We sought to characterize the $CD4^+$ T cell subsets expressing CCR5 and CCR2 to help us understand the organization and properties of what we presumed were highly differentiated T_{EM}-like cells.

The similarities in patterns of expression for CCR5 and CCR2 shown in Fig. 1*A* led us to analyze cells for coincident receptor expression. As shown in Fig. 1*B*, CCR2 is expressed principally on cells that also express CCR5. In data from 16 donors, the $CCR5^-CCR2^-$, $CCR5^+CCR2^-$, and $CCR5^+CCR2^+$ subsets constituted 67.6 ± 2.9, 25.2 ± 2.4, and 5.8 ± 0.9%, respectively, of $CD4^+CD45RO^+$ T cells. Their low frequency (1.4 ± 0.1% of $CD4^+$ $CD45RO^+$ T cells) and relatively dull staining for CCR2 made it difficult to purify significant numbers of the $CCR5^-CCR2^+$ cells reliably, and this subset was not analyzed further.

As compared with $CD62L^+$ cells, $CD62L^-$ cells have shorter telomeres (43) and fewer TREC (44). The patterns of expression of CCR5, CCR2, and CD62L (Fig. 1*A*, 1*B*, and Table I) suggested sequential induction of CCR5 followed by CCR2 during effector/memory cell differentiation. This hypothesis was supported by the decreasing numbers of TREC in going from naive ($CD45RO^-$), to $CCR5^-CCR2^-$, $CCR5^+CCR2^-$, and $CCR5^+CCR2^+$effector/memory ($CD45RO^+$) cells that had been purified from multiple donors (Fig. 1*C*). These data demonstrate that expression patterns for CCR5 and CCR2 reveal real differences in the subsets' histories, not simply heterogeneity in surface markers of cells that are otherwise identical, and suggest a generally unidirectional pathway of activation and increasing proliferation ending with the $CCR5^+CCR2^+$ subset.

Increasing memory character from $CCR5^-CCR2^-$ → $CCR5^+CCR2^-$ → $CCR5^+CCR2^+$ subsets

Given the data above, we analyzed the subsets defined by CCR5 and CCR2 for both phenotypic and functional correlates of differ-

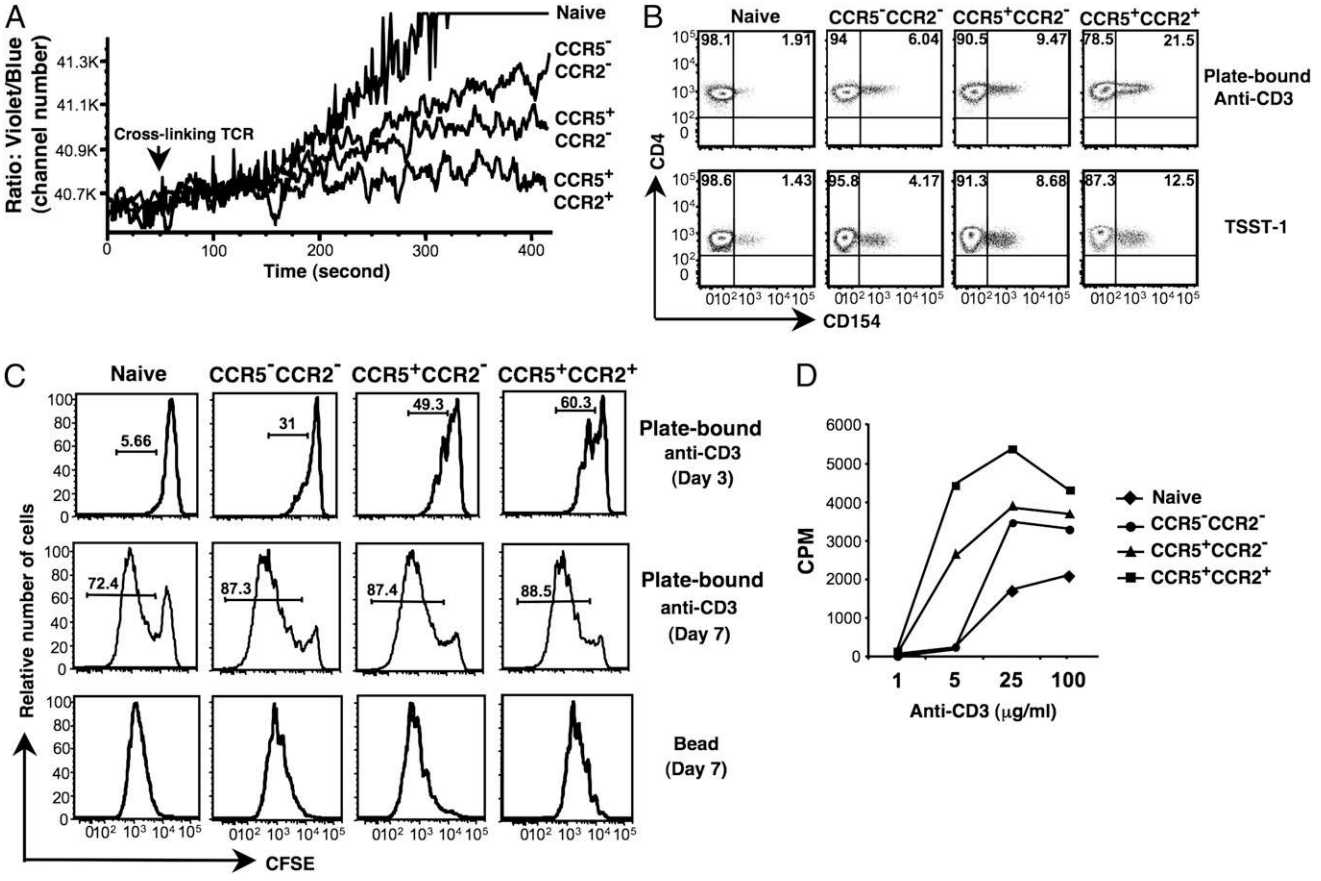

FIGURE 2. TCR responses become progressively more memory cell-like from the $CCR5^-CCR2^-$ to $CCR5^+CCR2^-$ to $CCR5^+CCR2^+$ subsets. *A*, For analyzing TCR-induced rises in intracellular calcium in naive cells, purified $CD4^+$ T cells were loaded with indo-1 AM ester and incubated with anti–CD4-allophycocyanin-Cy7, anti–CD45RO-PE-Cy5, and biotin-conjugated anti-CD3. For analyzing responses in effector/memory cells from the same donor and at the same time, $CD45RA^-$ $CD4^+$ T cells were purified, loaded with indo-1 AM ester, and incubated with anti–CD4-allophycocyanin-Cy7, anti–CD45RO-PE-Cy5, anti–CCR2-allophycocyanin, anti–CCR5-FITC, and biotin-conjugated anti-CD3. Ratios of 405/20 nm:525/20 nm emissions were measured before and after CD3 cross-linking by the addition of avidin. Data were analyzed using FlowJo. The response curve for naive ($CD45RO^-$) cells becomes flat where it exceeds the scale shown. Results are from one donor, representative of three. *B*, Purified $CD4^+$ T cells were sorted into naive ($CD45RO^-$) and the three $CD45RO^+$ subsets based on CCR5 and CCR2, and the subsets were activated by plate-bound anti-CD3 plus soluble anti-CD28 (*top row*) or TSST-1 (*bottom row*) for 6 h in the presence of anti–CD154-allophycocyanin. Quadrant boundaries for CD154 were set using nonactivated cells and cultures of activated cells from which anti-CD154 had been omitted. Results are from one donor, representative of five. *C*, Cells purified as in *B* were loaded with CFSE and activated by plate-bound anti-CD3 plus soluble anti-CD28 (*top and middle rows*) or by beads displaying anti-CD3 and anti-CD28 (*bottom row*) for either 3 or 7 d. Horizontal bars indicate cells that have proliferated and diluted CFSE, quantified as percent of total cells. After culturing for 7 d with beads, virtually all cells had diluted CFSE. Results are from one donor, representative of five. *D*, Cells purified as in *B* were cultured with various concentrations of plate-bound anti-CD3 plus soluble anti-CD28 for 2 d, after which cells were pulsed with 1 μCi [^{3}H]thymidine for 16 h. Cells were then harvested, and radioactivity was measured. Results are shown for absolute counts (CPM) and are from one donor, representative of three.

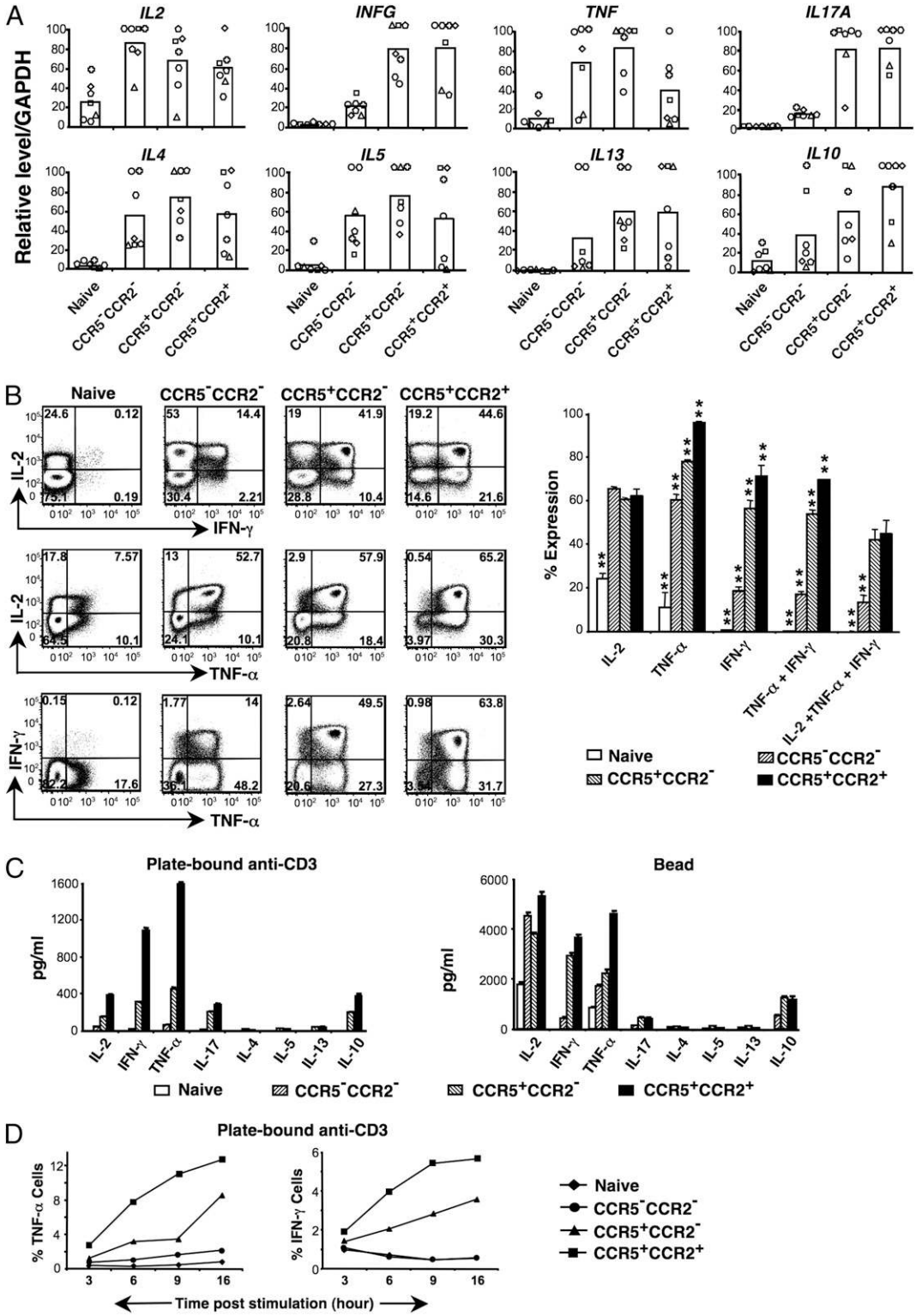

FIGURE 3. CCR5$^+$CCR2$^-$ and CCR5$^+$CCR2$^+$ subsets are enriched in cells that are able to produce effector cytokines. *A*, Purified CD4$^+$ T cells were sorted into naive (CD45RO$^-$) and the three CD45RO$^+$ subsets based on CCR5 and CCR2, the subsets were activated with PMA and ionomycin for 3 h, and relative levels of mRNAs were determined in duplicate using real-time RT-PCR and normalized to values for *GAPDH*. For each donor, represented by a unique symbol, the value for the cell subset containing the highest level of mRNA for a given cytokine was set at 100. The open bars show the means of the normalized values for each subset for each cytokine. Cells were purified from seven donors for measuring mRNA for *IL17A* and from a separate group of seven donors for measuring mRNAs for the other cytokines. *B*, Subsets were purified as in *A*, activated with PMA and ionomycin in the presence of monensin for 4 h and stained for intracellular cytokines using anti–IL-2-FITC, anti–IFN-γ-allophycocyanin, and anti–TNF-α-Alexa 700. For dot plots from a single donor (*left*), quadrant boundaries were set based on samples stained with all Abs except one, and numbers show percentages of cells in each quadrant. Bar graphs (*right*) show combined results from three donors for percentages of cells staining for individual and selected combinations of cytokines. Error bars show SEM. $^{**}p < 0.01$, compared with all other bars for that cytokine or cytokine combination, using a two-tailed Student *t* test. *C*, Subsets were purified as in *A* and activated by plate-bound anti-CD3 plus soluble anti-CD28 (*left panel*) or by beads displaying anti-CD3 and anti-CD28 (*right panel*). Cells were cultured at 1×10^6 cells/ml for 16 h before supernatants were collected for measuring cytokine concentrations by ELISA. Values

entiation. In addition to loss of expression of CD62L and CCR7, loss of CD27 and CD28 (34, 45, 46) has also been associated with progressive T cell differentiation. Although decreased in the CCR5$^+$CCR2$^-$ and CCR5$^+$CCR2$^+$ versus the naive and CCR5$^-$CCR2$^-$ cells, CCR7 and CD27 were not significantly different between the CCR5$^+$CCR2$^-$ and CCR5$^+$CCR2$^+$ subsets (Table I). Most of the CCR5$^+$CCR2$^-$ and CCR5$^+$CCR2$^+$ cells were CD27$^+$, and very few cells in any of the subsets lacked CD28. The data demonstrate that the subsets defined by CCR5 and CCR2 do not correspond in a simple way to those studied previously, using other markers of CD4$^+$ T cell differentiation. Previous data have shown that CCL2 recruits CD26^{bright} CD4$^+$ T cells in assays of transendothelial migration (47) and that, correspondingly, CCR2$^+$ CD4$^+$ T cells are CD26^{bright} (48). Consistent with these findings, we observed increasing levels of CD26 from CCR5$^-$CCR2$^-$ to CCR5$^+$CCR2$^-$ to CCR5$^+$CCR2$^+$ cells (Table I).

A number of biochemical and functional features distinguish effector/memory versus naive cells (49, 50). Paradoxically, given their generally enhanced biological responses, memory cells show diminished downstream signaling, including a smaller rise in intracellular calcium after TCR activation, compared with naive cells (44, 50–52). As shown in Fig. 2*A*, there was a progressive fall in the TCR-mediated calcium signal from the naive to CCR5$^-$CCR2$^-$ to CCR5$^+$CCR2$^-$ to CCR5$^+$CCR2$^+$ cells. We next analyzed thresholds and rapidity of activation by exposing the T cell subsets to plate-bound OKT3 (anti-CD3) and soluble anti-CD28, or the more potent stimuli of bead-bound OKT3 (anti-CD3) and anti-CD28 or TSST-1 superantigen. As shown in Fig. 2*B*, within 6 h of culturing with plate-bound anti-CD3 and soluble anti-CD28 or with TSST-1, some cells can be seen to have upregulated CD154 (CD40L), and there was a progressive increase in percentage of CD154$^+$ cells from the naive to CCR5$^-$CCR2$^-$ to CCR5$^+$CCR2$^-$ to CCR5$^+$CCR2$^+$ subsets. With regard to responses to TSST-1, we found no significant differences in percentages of Vβ2$^+$ cells among the subsets (data not shown). Analyzing CFSE-loaded cells at day 3 of activation with plate-bound anti-CD3 and soluble anti-CD28, we also found successively higher percentages of proliferated cells from the naive to CCR5$^-$CCR2$^-$ to CCR5$^+$CCR2$^-$ to CCR5$^+$CCR2$^+$ subsets (Fig. 2*C*). By day 7, few differences were observed among the effector/memory subsets in the percentages of cells that had proliferated, and after 7 d of activation using bead-bound anti-CD3 and anti-CD28, we found that, if anything, the naive and CCR5$^-$CCR2$^-$ subsets had proliferated best.

In another way of assaying for proliferation threshold, we performed a dose response to plate-bound anti-CD3 and measured incorporation of [^{3}H]thymidine after 2 d. As shown in Fig. 2*D*, there was increasing sensitivity to TCR cross-linking from the naive to CCR5$^-$CCR2$^-$ to CCR5$^+$CCR2$^-$ to CCR5$^+$CCR2$^+$ subsets, and the CCR5$^+$CCR2$^+$ subset reached a plateau at the lowest concentration of anti-CD3. Together, these data demonstrate a positive gradient with regard to rapidity of and sensitivity to TCR-mediated activation and proliferation in going from the naive to CCR5$^-$CCR2$^-$ to CCR5$^+$CCR2$^-$ to CCR5$^+$CCR2$^+$ cells.

Increasing, rapid effector capability from CCR5$^-$CCR2$^-$ → CCR5$^+$CCR2$^-$ → CCR5$^+$CCR2$^+$ subsets

Because the ability to produce certain cytokines rapidly after activation is a hallmark of CD4$^+$ memory cells, we analyzed levels of mRNAs for a number of cytokines in the naive and three effector/memory subsets from multiple donors following activation ex vivo with PMA and ionomycin. As shown in Fig. 3*A*, the CCR5$^+$CCR2$^-$ and CCR5$^+$CCR2$^+$ subsets showed relatively high levels of mRNAs for Th1-, Th2-, and Th17-type cytokines. For *IFNG*, *IL10*, *IL13*, and *IL17A*, these subsets showed levels higher than in the CCR5$^-$CCR2$^-$ effector/memory subset. Levels for the other cytokine mRNAs were comparable among the three effector/memory subsets, with the exception of mRNA for *TNF*, which was in general lower in the CCR5$^+$CCR2$^+$ cells. In analyzing IL-2, IFN-γ, and TNF-α by intracellular staining, we found an increase in IL-2 production in the effector/memory versus naive populations but no differences among the memory subsets, whereas there was a gradient of increasing frequencies of IFN-γ^+ and TNF-α^+ cells in going from the naive to CCR5$^-$CCR2$^-$ to CCR5$^+$CCR2$^-$ to CCR5$^+$CCR2$^+$ cells (Fig. 3*B*). The pattern of increasing staining for TNF-α was at odds with the mRNA data, suggesting a posttranscriptional contribution to the production of TNF-α that differs among the subsets. Posttranscriptional control of TNF-α production has been well described (53).

We also assayed cells for cytokine secretion after stimulation for 1 d with plate-bound OKT3 plus soluble anti-CD28 or bead-bound OKT3 and anti-CD28. Consistent with the patterns of activation shown in Fig. 2*B–D*, the CCR5$^+$CCR2$^+$ subset secreted much greater amounts of cytokines after 1 d of stimulation with plate-bound OKT3 plus soluble anti-CD28 (Fig. 3*C*, *left panel*). With use of the stronger stimulus of bead-bound OKT3 and anti-CD28 (Fig. 3*C*, *right panel*), the pattern of cytokine secretion corresponded more closely to the results of intracellular staining after stimulation with PMA and ionomycin, as shown in Fig. 3*B*. To evaluate better the rapidity of cytokine production, we performed a time course of percentages of cytokine-producing cells after activation with plate-bound anti-CD3. As shown in Fig. 3*D*, by 6 h the CCR5$^+$CCR2$^+$ subset already contained higher percentages of cytokine-producing cells than did the other subsets. Together, the data in Figs. 2 and 3 suggest that the CCR5$^+$CCR2$^+$ cells would be prepared for early and rapid effector responses after re-encountering Ags.

Increasing responsiveness to survival cytokines from CCR5$^-$CCR2$^-$ → CCR5$^+$CCR2$^-$ → CCR5$^+$CCR2$^+$ subsets

Responses to IL-7 and IL-15, cytokines important for memory cell survival, have been reported to increase with increasing differentiation among CD4$^+$ T cells (33). As shown in Fig. 4*A*, culturing with IL-7 and/or IL-15 resulted in increasing percentages of proliferated cells in going from the naive to CCR5$^-$CCR2$^-$ to CCR5$^+$CCR2$^-$ to CCR5$^+$CCR2$^+$ subsets. In analyzing receptors for IL-15 and IL-7 (Fig. 4*B*), we found progressive increases in expression of CD122 (IL-2Rβ) and CD132 (IL-2Rγ) from the naive to CCR5$^-$CCR2$^-$ to CCR5$^+$CCR2$^-$ to CCR5$^+$CCR2$^+$ subsets.

The pattern of expression for CD127 (IL-7Rα) was more complex (Fig. 4*B*). Intermediate levels with a normal distribution were found on naive cells, with the memory subsets becoming increasingly bimodal. The highest percentage of CD127$^-$ cells was found in the CCR5$^+$CCR2$^-$ subset. Analyzing intensities of staining specifically on the CD127$^+$ cells also showed increasing levels of CD127 from the naive to CCR5$^-$CCR2$^-$ to CCR5$^+$CCR2$^-$ to CCR5$^+$CCR2$^+$ subsets. Uniformly, across multiple donors,

are means of duplicate measurements of single samples. Error bars show SEM. Results are from one donor, representative of four. *D*, Subsets were purified as in *A*, activated by plate-bound anti-CD3 plus soluble anti-CD28 in the presence of monensin, harvested at various times, and stained for intracellular cytokines using anti–IFN-γ-allophycocyanin and anti–TNF-α-Alexa 700. Results were analyzed as in *B* and are shown as percentages of cytokine-positive cells. Results are from one donor, representative of three.

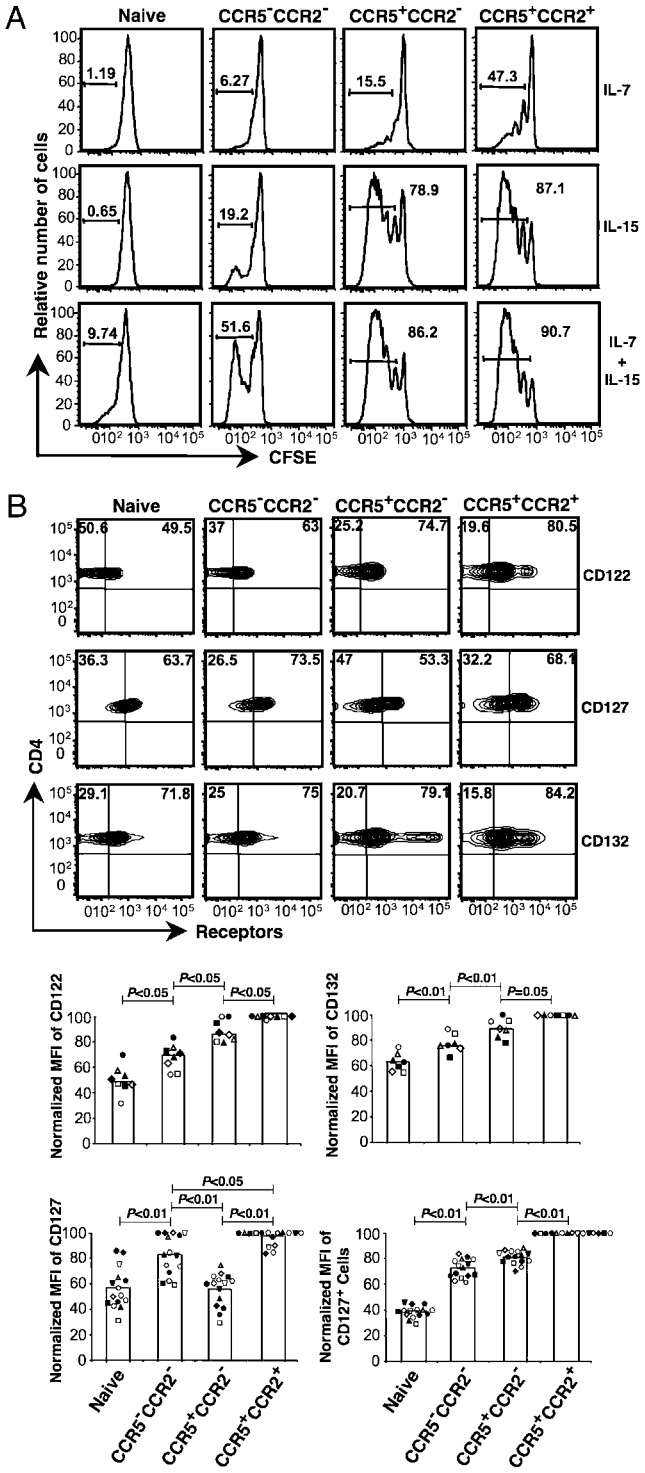

FIGURE 4. Increasing response to, and expression of receptors for, IL-7 and IL-15 from the naive to $CCR5^-CCR2^-$ to $CCR5^+CCR2^-$ to $CCR5^+CCR2^+$ subsets. *A*, Purified $CD4^+$ T cells were sorted into naive ($CD45RO^-$) and the three $CD45RO^+$ subsets based on CCR5 and CCR2, loaded with CFSE, and cultured for 7 d in the presence of 25 ng/ml each of IL-7 and/or IL-15. Horizontal bars indicate cells that have proliferated and diluted CFSE, quantified as percent of total cells. Results are from one donor, representative of three. *B*, Purified $CD4^+$ T cells were stained with anti–CD4-FITC, anti–CD45RO-PE-Cy7, anti–CCR5-PE-Cy5, anti–CCR2-allophycocyanin, and one of the three Abs: anti–CD127-PE, anti–CD122-PE, or anti–CD132-PE. For the contour plots (*top panels*), quadrant boundaries for the cytokine receptors were set based on samples stained with all Abs except either anti-CD127, anti-CD122, or anti-CD132. Results are from one donor, representative of seven. In the *bottom panels* are shown median fluorescent intensities of staining for CD122, CD132, and CD127 within the naive ($CD45RO^-$) and the three $CD45RO^+$ subsets. For CD127, the median fluorescent intensities are also shown only for cells falling within the $CD127^+$ gate. For each donor, represented by a unique symbol, the value for the cell subset showing the highest MFI for a given receptor was set at 100. Open bars show means of the normalized values. For comparisons shown by the horizontal bars above the symbols, *p* values were determined using the Wilcoxon matched-pairs signed-rank test.

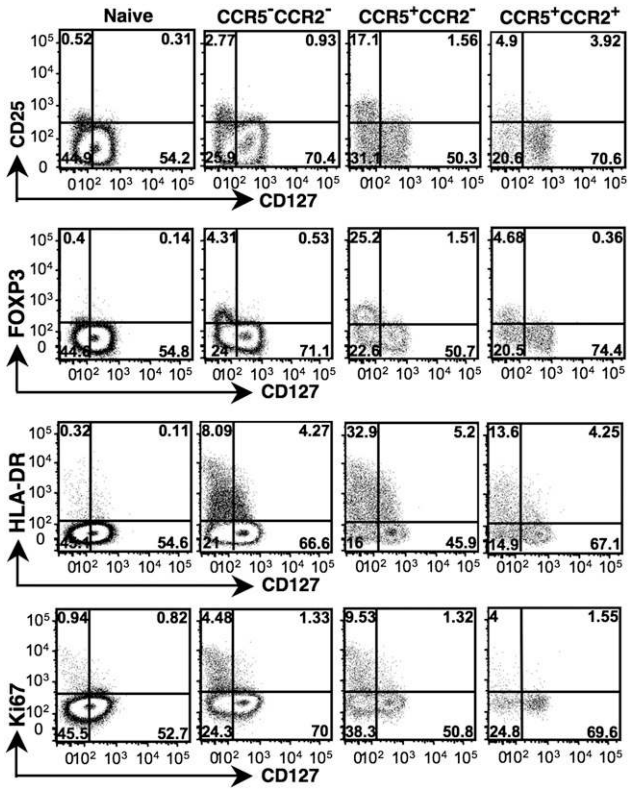

FIGURE 5. The $CCR5^+CCR2^-$ subset is enriched in $FOXP3^+$, activated, and proliferating cells. $CD4^+$ T cells were purified and some were stained with anti–CD4-allophycocyanin-Cy7, anti–CD45RO-PE-Cy7, anti–CCR5-PE-Cy5, anti–CCR2-biotin plus streptavidin-PE, and anti–CD127-allophycocyanin and either anti–HLA-DR-FITC or, after being fixed and permeabilized, anti–Ki67-FITC. Other cells were stained with anti–CD4-FITC, anti–CD45RO-PE-Cy7, anti–CCR5-PE-Cy5, anti–CCR2-biotin plus streptavidin-PE, and anti–CD127-allophycocyanin, and either anti–CD25-allophycocyanin-Cy7 or, after being fixed and permeabilized, anti–FOXP3-Alexa Fluor 700. For the $CCR5^-CCR2^-$, $CCR5^+CCR2^-$, and $CCR5^+CCR2^+$ plots, only $CD45RO^+$ cells are shown. Quadrant boundaries were set based on samples stained with all Abs except one. Results are from 1 donor, representative of >10 donors using these same Abs for staining, although with various combinations of fluorescent conjugates.

the cells with the highest levels of CD127 were found in the $CCR5^+CCR2^+$ subset. Because CD127 is downregulated after exposure to IL-7 and related cytokines, and levels of CD127 on freshly isolated T cells have been reported to reflect, in part, exposure to IL-7 in vivo (54), we analyzed CD127 on purified T cell subsets following overnight culture. Despite some increase in staining on the naive cells after culturing, the relative levels of CD127 were unchanged (data not shown).

CD127 is absent from human $FOXP3^+$ T cells and profoundly downregulated after TCR activation (30, 55–58). Therefore, we analyzed the naive and three effector/memory subsets for expression of the transcription factor FOXP3, activation markers

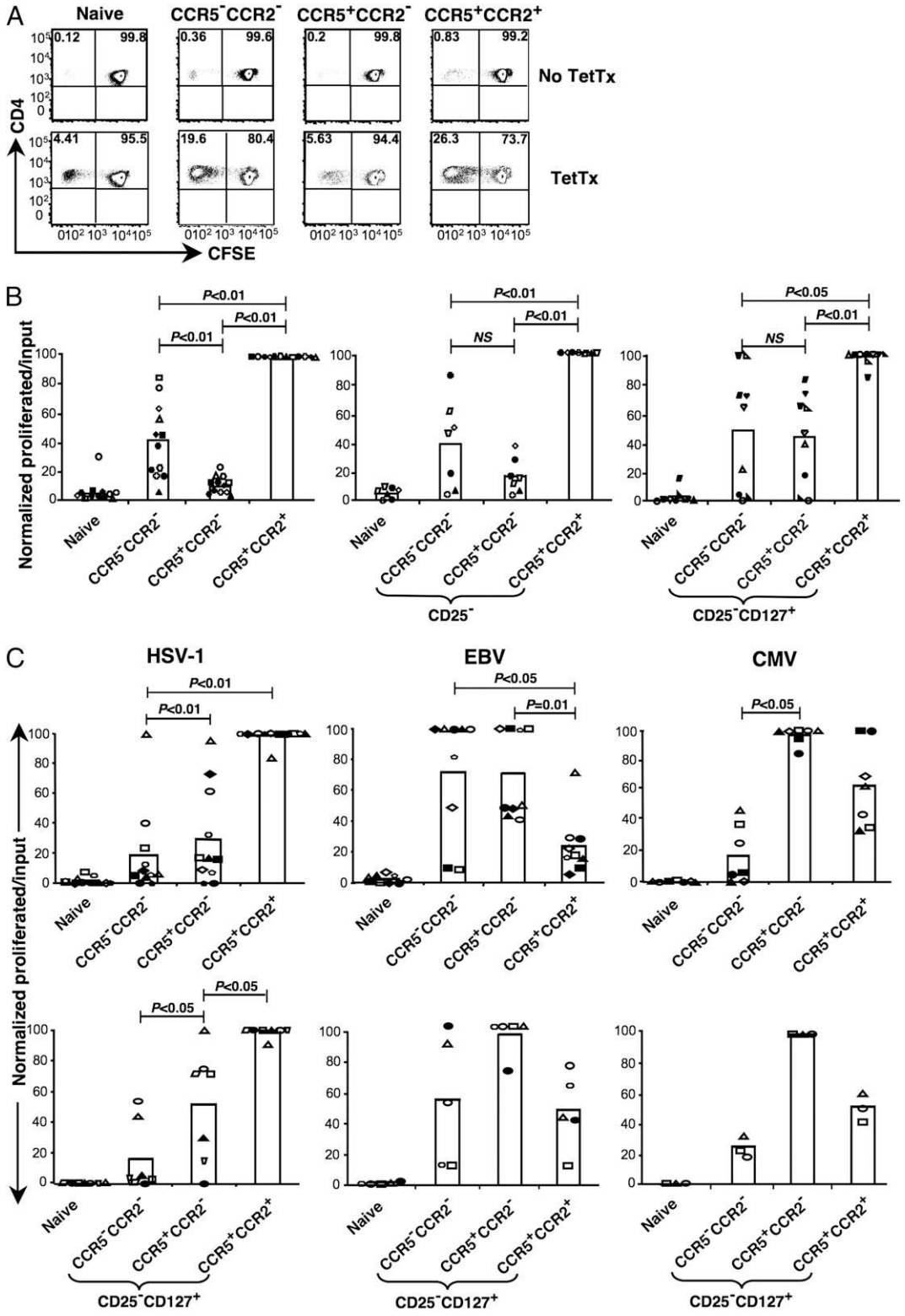

FIGURE 6. Differing patterns of response to long absent versus persistent Ags among effector/memory subsets. *A*, Purified $CD4^+$ T cells were sorted into naive ($CD45RO^-$) and the three $CD45RO^+$ subsets based on CCR5 and CCR2, and cells were loaded with CFSE and cultured with autologous, dodecyldimethylamine oxide (DDAO)-loaded, irradiated PBMCs, in either the absence or presence of tetanus toxoid. On day 7, cells were stained with anti–CD3-allophycocyanin-Cy7, anti–CD4-PE, and PI. $CD3^+CD4^+DDAO^-PI^-$ cells are displayed. Numbers show percentages of cells in each quadrant. Dot plots are from 1 donor, representative of >10. *B*, Purified $CD4^+$ T cells were sorted into naive ($CD45RO^-$) and the three $CD45RO^+$ subsets based on CCR5 and CCR2, without or with additionally limiting the collection of the $CD45RO^+$ cells to those that were $CD25^-$ or $CD25^-CD127^+$. Cells were cultured and analyzed as in *A*, except that absolute cell numbers were determined by adding fluorescent beads to each sample. Numbers of $CFSE^{low/-}$ cells in the tetanus toxoid cultures were corrected for numbers of input cells in each sample (day 0). For each donor, represented by a unique symbol, the value for the cell subset showing the highest ratio of $CFSE^{low/-}$/input cells was set at 100. Some donors overlap among the three panels, as indicated by the symbols, but most do not. As in *A*, no significant responses were seen in the cells cultured without tetanus toxoid (data not shown). The open bars show the mean values for each subset. For comparisons shown by the horizontal bars above the symbols, *p* values were determined using the Wilcoxon matched-pairs signed-rank

CD25 and HLA-DR, and the proliferation-associated nuclear Ag, Ki67 (Fig. 5, Table I). FOXP3 is expressed generally, but transiently, after activation of human T cells (59), as well as in human regulatory T cells (Tregs) (60, 61). The cells expressing DR and/or CD25 and/or Ki67 and/or FOXP3 were all enriched within the $CCR5^+CCR2^-$ subset. Together, these data indicate that the $CCR5^+CCR2^-$ subset contains disproportionate numbers of Tregs and activated/cycling cells.

These findings raised the issue of how activated cells and Tregs might have affected the differences among the effector/memory subsets in functional assays for TCR-induced proliferation and cytokine production. We therefore repeated the dose response to plate-bound anti-CD3 and the intracellular staining for cytokine production after removing cells that were $CD25^+$ and/or $CD127^-$. Eliminating the $CD25^+$ and/or $CD127^-$ cells removed all the cells that were $FOXP3^+$ cells and the vast majority of additional cells that were DR^+ and $Ki67^+$ (Fig. 5 and data not shown), i.e., Tregs plus recently activated cells. As shown in Supplemental Fig. 1, removing these cells did not change the relationships among the subsets. The gradients in sensitivity to TCR-mediated activation and in percentages of cells capable of making TNF-α and/or IFN-γ were maintained in going from naive to $CCR5^-CCR2^-$ to $CCR5^+CCR2^-$ to $CCR5^+CCR2^+$ cells.

Responses to vaccine and viral Ags differ among $CCR5^-CCR2^-$, $CCR5^+CCR2^-$, and $CCR5^+CCR2^+$ subsets

To analyze Ag-specific responses among the effector/memory subsets, we measured numbers of proliferated cells after culturing with tetanus toxoid (Fig. 6*A*, 6*B*). In every case, across multiple donors, the rank order of the subsets for numbers of proliferated cells was $CCR5^+CCR2^+ > CCR5^-CCR2^- > CCR5^+CCR2^-$. We considered, based on the staining profiles for FOXP3 and activation markers shown in Fig. 5 and Table I, whether differences in tetanus toxoid responses could be due principally to differences in numbers of Tregs and recently activated cells among the subsets. These cells could affect frequencies of Ag-responsive cells through suppressor activity as well as through simple dilution in case the recently activated cells lacked cells responding to tetanus toxoid. We tested this possibility by performing the tetanus toxoid cultures with subsets depleted of either $CD25^+$ cells only, or depleted of both $CD25^+$ and $CD127^-$ cells. CD25 depletion was relatively specific for $FOXP3^+$ cells—>75% of $CD25^+$ cells were also $FOXP3^+$ (and ~70% of the $FOXP3^+$ cells were $CD25^+$)—whereas the additional depletion of $CD127^-$ removed the remaining $FOXP3^+$ and activated cells, including, presumably, any of the small numbers of recently described Tr1-like cells (see above and Ref. 58). As shown in Fig. 6*B*, depleting $CD25^+$ cells had a modest effect in increasing the relative response within the $CCR5^+CCR2^-$ subset. Nonetheless, the increased responses after removing $CD25^+$ cells could not be accounted for solely by a small enrichment in reactive cells, demonstrating the presence of suppressor activity within the $CD25^+$ population (data not shown). Further depletion of the $CD127^-$ cells had an additional effect in diminishing relative differences among the subsets (Fig. 6*B*), and brought the responses in the $CCR5^+CCR2^-$ cells equal to those in the $CCR5^-CCR2^-$ cells.

We next analyzed responses among the subsets to extracts of cells infected with herpesviruses, which produce life-long, latent infections. For HSV-1 and EBV, ~70% of donors had $CD45RO^+$ cells that responded, whereas for CMV, responses were found in ~50% of donors (data not shown). Results for each virus for all responding donors are shown in Fig. 6*C*. For HSV-1, as for tetanus toxoid, the $CCR5^+CCR2^+$ subset showed the greatest responses. By contrast, for EBV, maximal responses were seen in the $CCR5^-CCR2^-$ and $CCR5^+CCR2^-$ subsets, whereas for CMV the $CCR5^+CCR2^-$ cells typically showed the greatest responses. In some experiments, we cultured only the $CD25^-CD127^+$ cells in each subset—again, to remove suppressor and recently activated cells. The result was to increase responses among the $CCR5^+CCR2^-$ cells disproportionately, although the effect of removing the $CD25^+$ and $CD127^-$ cells was smallest in responses to CMV.

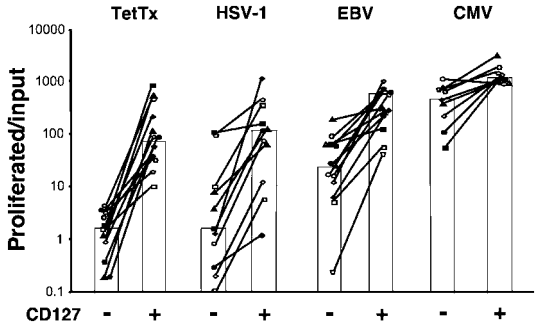

FIGURE 7. Agent-dependent differences in levels of response in $CD127^-$ versus $CD127^+$ effector/memory $CD4^+$ T cells. Purified $CD4^+CD45RO^+CD25^-CD127^-$ and $CD4^+CD45RO^+CD25^-CD127^+$ cells were cultured and analyzed as in Fig. 6. Numbers are $CFSE^{low/-}$/input cells × 100, and for each of the four agents, each donor is represented by a unique symbol; results are shown for all responding donors, i.e., all donors that had responses within the $CD127^+CD25^-$ cells. No donors had responses limited to $CD25^-CD127^-$ cells. Lines connect values from the two cell subsets for a given donor. The open bars show the median values among the donors within the cell subsets for each agent.

Although these data showed that levels of response to tetanus toxoid and herpesviruses could be enhanced by removing suppressor and recently activated cells, the data also suggested significant differences in the magnitudes of such effects, depending on the Ag/agent. To analyze cells in the resting state versus recently activated cells more directly, we measured responses to tetanus toxoid and the three herpesviruses in the $CD45RO^+$ population within total $CD25^-CD127^-$ and $CD25^-CD127^+$ cells, without separating cells based on CCR5 and CCR2. As shown in Fig. 7, there were no or only low-level responses to tetanus toxoid in the $CD127^-$ cells, even though these cells had been partially depleted of Tregs by removing the $CD25^+$ population. Responses in the $CD25^-CD127^-$ cells showed the rank order CMV > EBV > HSV-1 > tetanus toxoid, and, similarly, relationships between levels of response in $CD25^-CD127^-$ versus $CD25^-CD127^+$ cells differed among the agents. It is also of note that, for a given agent, we did not see a consistent correlation from donor to donor in the magnitude of the responses among $CD25^-CD127^-$ versus $CD25^-CD127^+$ cells; Fig. 7 shows crossed lines in responses to individual agents.

Increased susceptibility to death in the $CCR5^+CCR2^-$ subset

As defined by CCR7 and other markers, human $CD4^+$ T_{EM} cells, compared with T_{CM} and naive cells, have been shown to be more

test. *C*, Cells were purified, cultured, and analyzed as in *B*, except that culturing was done with extracts from virus-infected cells instead of tetanus toxoid. In the lower panels, the collection of $CD45RO^+$ cells was limited to those that were $CD25^-CD127^+$. Some, but not all, donors overlap between *top* and *bottom panels*, as indicated by the symbols. Control extracts from noninfected cells gave no responses (data not shown). We applied the Wilcoxon matched-pairs signed-rank test to normalized values from multiple donors, but $p < 0.05$ cannot be reached using this test on fewer than six pairs of numbers.

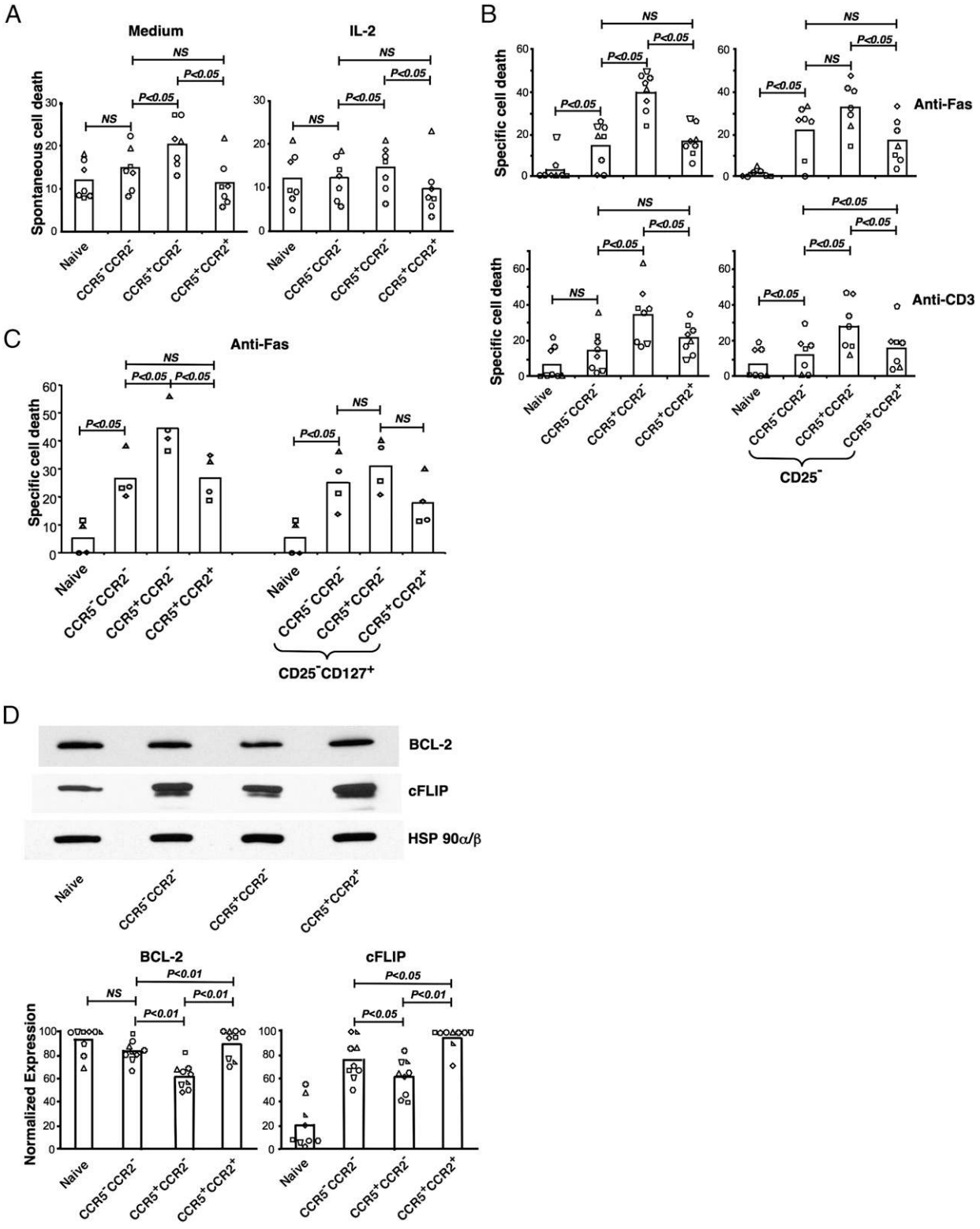

FIGURE 8. CCR5$^+$CCR2$^-$ cells are most susceptible to apoptosis. *A*, Purified CD4$^+$ T cells were sorted into naive (CD45RO$^-$) and the three CD45RO$^+$ subsets based on CCR5 and CCR2. Before and after culturing for 16 h, viable cells were identified by flow cytometry, and cell numbers were determined by adding fluorescent beads to each sample. Percentages of cells dying in medium alone or with medium containing IL-2 were calculated as [(1 − (live cells at 16 h/live cells at 0 h) × 100]. Each donor is represented by a unique symbol, and the same donors were used for the *left* and *right panels*. Open bars show the mean values for each cell subset. For comparisons shown by the horizontal bars above the symbols, *p* values were determined using the Wilcoxon matched-pairs signed-rank test. *B*, Purified CD4$^+$ T cells were sorted as in *A*, either including or excluding cells that were CD25$^+$. In the *top panels*, cells were incubated without or with anti-Fas plus anti-mouse IgG_3. In the *lower panels*, cells were incubated without or with plate-bound anti-CD3 plus soluble anti-CD28. Percentage-specific cell death was calculated as [1− (live cells treated/live cells untreated) × 100]. For the data shown, live cells were identified based on scatter profiles. In some experiments not shown, live cells were also identified after staining with PI and annexin V, resulting in somewhat lower numbers of live cells, but similar rank orders in specific death among the subsets. The *x*-axis labels on the lower panels apply also to the upper panels. Each donor is represented by a unique symbol, and most but not all donors overlap between the *left* and *right panels* for anti-Fas and anti-CD3 experiments, as

susceptible to apoptosis (33–35), suggesting that progressive differentiation is associated with greater instability among T cell subsets. We investigated cell death within the naive and three memory subsets ex vivo, either "spontaneous" death or death following cross-linking Fas or CD3/CD28. Under all conditions, death was greatest in the $CCR5^+CCR2^-$ subset (Fig. 8). In the case of spontaneous death, adding IL-2 to the overnight culture preferentially diminished death in the $CCR5^+CCR2^-$ cells, although not fully to the levels in the other subsets (Fig. 8*A*). Because $CD25^+$ (Treg) cells are highly susceptible to Fas-mediated apoptosis (62) and the $CCR5^+CCR2^-$ subset is particularly enriched in these cells, we also analyzed Fas- and CD3-mediated death in the subsets after depleting $CD25^+$ cells. As shown in Fig. 8*B*, removing the $CD25^+$ cells decreased death preferentially in the $CCR5^+CCR2^-$ subset, but did not completely eliminate differences between the $CCR5^+CCR2^-$ and other subsets. In a smaller number of donors, we also tested Fas cross-linking after removing both $CD25^+$ and $CD127^-$ cells, and, again, differences between the $CCR5^+CCR2^-$ and other subsets were diminished (Fig. 8*C*).

cFLIP and BCL-2 are inhibitors of apoptosis, acting principally within the extrinsic and intrinsic pathways, respectively (63), and maintaining levels of BCL-2 is an important mechanism underlying the trophic effects of IL-7 on T cells (64). As shown in Fig. 8*D*, we found that the $CCR5^+CCR2^+$ subset had higher levels of cFLIP and BCL-2, compared with the $CCR5^+CCR2^-$ subset, and that, in general, the $CCR5^+CCR2^-$ subset also contained lower levels of cFLIP and BCL-2, compared with the $CCR5^-CCR2^-$ cells. Quantification of results from multiple donors by densitometry showed that these differences were significant (Fig. 8*D*, *lower panel*). Together, these data provide molecular correlates of, and potential explanations for, differences among the subsets in their propensities to die, and demonstrate that $CCR5^+CCR2^+$ cells are less susceptible to apoptosis than are $CCR5^+CCR2^-$ cells and not significantly more susceptible than are the less differentiated $CCR5^-CCR2^-$ cells.

CCR7 expression is not an important determinant of the functional differences among the $CCR5^-CCR2^-$, $CCR5^+CCR2^-$, and $CCR5^+CCR2^+$ subsets

T_{CM} and T_{EM} were initially defined based on the expression of CCR7 (16), and $CCR7^-$ cells were identified as the effector-capable population. It was of interest, therefore, to investigate the role of $CCR7^+$ versus $CCR7^-$ cells in the behaviors of the $CCR5^-CCR2^-$, $CCR5^+CCR2^-$, and $CCR5^+CCR2^+$ subsets. Fig. 9*A* shows staining within the $CCR5^-CCR2^-$, $CCR5^+CCR2^-$, and $CCR5^+CCR2^+$ subsets for CCR7 as well as for CD62L, which, as described above, has also been used to distinguish T_{CM} from T_{EM}. Consistent with data on the individual markers from multiple donors in Table I, $CCR5^+CCR2^-$ and $CCR5^+CCR2^+$ cells have similar percentages of $CCR7^+$ cells, although significantly lower than in the $CCR5^-CCR2^-$ (and naive) subsets, and the percentage of $CD62L^+$ cells declines progressively from the naive to the $CCR5^+CCR2^+$ subsets.

We divided the $CCR5^-CCR2^-$, $CCR5^+CCR2^-$, and $CCR5^+CCR2^+$ subsets further, based on the expression of CCR7, and tested the purified cells for sensitivity to activation by plate-bound anti-CD3. As shown in Fig. 9*B*, there was a gradient in percentages of cells upregulating CD154 from the $CCR5^-CCR2^-$ to $CCR5^+CCR2^-$ to $CCR5^+CCR2^+$ subsets, similar to the data in Fig. 2*B*, regardless of whether cells were $CCR7^+$ or $CCR7^-$. We also analyzed the relationship of CCR7 expression to the ability to produce TNF-α and/or IFN-γ. As shown in Fig. 9*C*, although within each subset, as compared with the $CCR7^+$ cells, the $CCR7^-$ cells contained higher percentages of cytokine producers, a gradient of cytokine production from the $CCR5^-CCR2^-$ to $CCR5^+CCR2^-$ to $CCR5^+CCR2^+$ subsets was found within both the $CCR7^+$ and $CCR7^-$ subpopulations. Together, these data suggest that the acquisition of CCR5 and CCR2 expression is associated with progressive differentiation of effector/memory $CD4^+$ T cells independently of the loss of CCR7.

$CCR5^+CCR2^+$ cells are highly armed

We considered whether cells expressing CCR2 might coexpress other inflammatory chemokine receptors in addition to CCR5. As shown in Fig. 10*A* and Table I, the majority of the $CCR2^+$ cells also expressed each of CXCR3, CCR6, and CCR4, whereas CCR2 showed a negative correlation with CCR7 and another compartment-specific, homeostatic receptor, CXCR5. As revealed by staining cells simultaneously for CCR2, CCR5, CXCR3, CCR6, and CCR4, some of the $CCR2^+$ cells coexpress all of the four additional receptors. Of the cells expressing each individual receptor that coexpress the additional four receptors, the $CCR2^+$ subset had the highest percentage of cells expressing all the receptors, and the $CCR4^+$ subset the lowest (Fig. 10*B*). Fig. 10*B* shows a general inverse correlation between total percentages of $CD4^+CD45RO^+$ cells that express a given receptor and the percentages of cells with that receptor that coexpress the four additional receptors. This pattern is consistent with a stochastic process in which receptors with the most restrictive requirements for induction during memory cell differentiation are found on cells that have undergone longer periods and/or multiple rounds of activation, which would presumably increase the chances that the cell encounters the conditions needed for receptor expression. In that case, $CCR2^+$ cells would likely have undergone more cell divisions and accumulated the other receptors, whose requirements for induction are less stringent, in line with our observations. We would also expect that only a small percentage of the $CCR2^+$ cells would express CCR2 alone and that, although, the $CCR2^+$ cells would show a shift toward multiple receptor expression, the $CCR4^+$ subset would be dominated by cells coexpressing relatively few receptors. Patterns for the subsets of cells expressing CCR6, CXCR3, and CCR5 would fall between those for CCR4 and CCR2. This was in fact the case, as seen in Supplemental Fig. 2, where we show the combined results for all the receptor combinations from 10 donors.

The data on receptor expression predicted that the $CCR5^+CCR2^+$ cells would respond to a broad array of chemokines. Fig. 10*C*, *left*

indicated by the symbols. Open bars show the mean values for each cell subset. For comparisons shown by the horizontal bars above the symbols, *p* values were determined using the Wilcoxon matched-pairs signed-rank test. *C*, Purified $CD4^+$ T cells were sorted as in *A*, either including or excluding cells that were $CD25^+$ and/or $CD127^-$. The cells were treated and the results were analyzed and presented as in *B*, except that *p* values were determined using one-way ANOVA applied to matched sets with Bonferroni posttest correction. *D*, Purified $CD4^+$ T cells were sorted into naive ($CD45RO^-$) and the three $CD45RO^+$ subsets based on CCR5 and CCR2. Cells were lysed, and 10 μg protein was loaded per lane for separation by SDS-PAGE and immunoblotting. Separate blots were probed for cFLIP and BCL-2, and each blot was probed for HSP 90α/β, demonstrating equal loading per lane. The *top panel* shows two blots from one donor, with results for HSP 90α/β shown for only one of the blots. The *bottom panel* shows quantification of BCL-2 and cFLIP bands by densitometry normalized to HSP 90α/β for each lane from each donor, represented by a unique symbol. For each donor the value for the BCL-2 or cFLIP band with the highest density was set at 100. The open bars show the mean value for each subset. For comparisons shown by the horizontal bars above the symbols, *p* values were determined using the Wilcoxon matched-pairs signed-rank test.

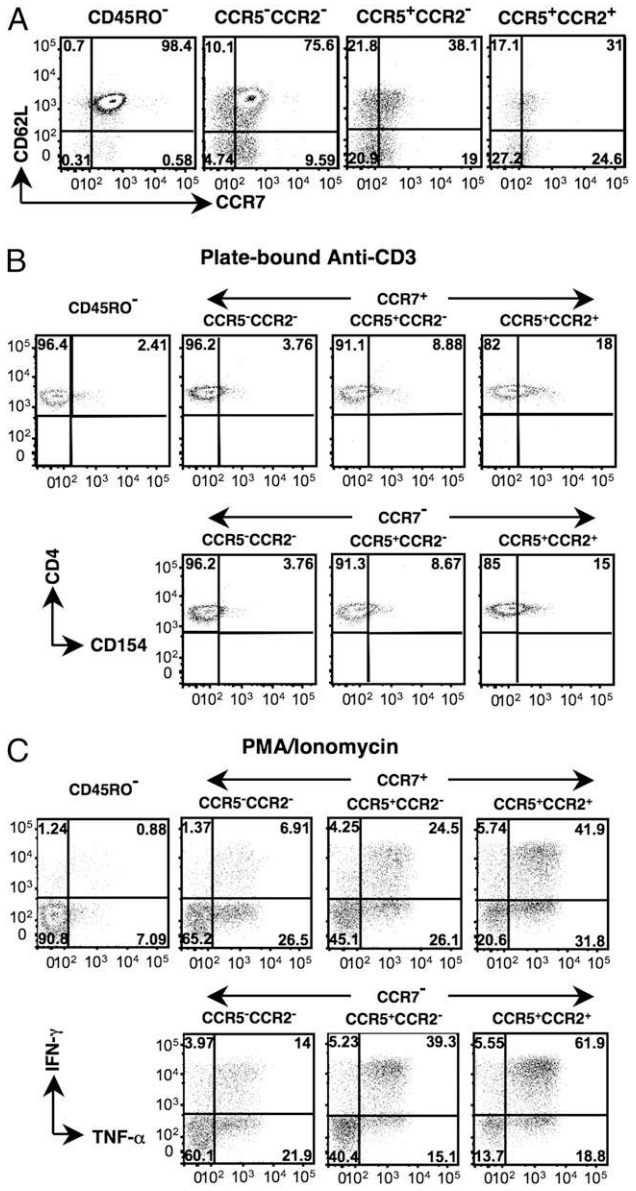

FIGURE 9. Features of increasing differentiation from the $CCR5^-CCR2^-$ to $CCR5^+CCR2^-$ to $CCR5^+CCR2^+$ subsets are found for both $CCR7^+$ and $CCR7^-$ cells. *A*, Purified $CD4^+$ T cells were stained with anti–CD4-allophycocyanin-Cy7, anti–CD45RO-PE-Cy7, anti–CCR5-PE-Cy5, anti–CCR2-biotin plus streptavidin-PE, anti–CD62L-allophycocyanin, and anti–CCR7-FITC. Only $CD4^+$ cells are shown. For the $CCR5^-CCR2^-$, $CCR5^+CCR2^-$, and $CCR5^+CCR2^+$ plots, only $CD45RO^+$ cells are shown. Quadrant boundaries were set based on samples stained with all Abs except one. Results are from one donor, representative of five. *B*, Purified $CD4^+$ T cells were sorted into naive ($CD45RO^-$) and the six $CD45RO^+$ subsets based on CCR5, CCR2, and CCR7, and the subsets were activated by plate-bound anti-CD3 plus soluble anti-CD28 for 6 h in the presence of anti–CD154-allophycocyanin, as in Fig. 2*B*. Quadrant boundaries for CD154 were set using nonactivated cells and cultures of activated cells from which anti-CD154 had been omitted. Results are from one donor, representative of three. *C*, Cells were purified as in *B*, activated with PMA and ionomycin in the presence of monensin for 4 h, and stained for intracellular cytokines, using anti–IFN-γ-allophycocyanin and anti–TNF-α-Alexa 700, as in Fig. 3*B*. Quadrant boundaries were set based on samples stained with all Abs except one. Results are from one donor, representative of four.

panel, shows results of chemotaxis experiments for the naive and three effector/memory subsets in response to chemokines specific for the relevant receptors. CXCL12 served as a positive control, because CXCR4 is expressed on cells in all $CD4^+$ T cell subsets (Table I). The three effector/memory subsets responded to CXCL9/MIG, ligand for CXCR3; CCL20/MIP-3α, ligand for CCR6; and CCL17/TARC, ligand for CCR4. In addition, the two $CCR5^+$ subsets migrated to CCL4/MIP-1β, and only the $CCR5^+CCR2^+$ subset migrated to CCL2/MCP-1. The expression of multiple functional chemokine receptors on the $CCR5^+CCR2^+$ cells suggested that they might migrate best to complex mixtures of proinflammatory chemokines that are produced by TLR activation. As shown in Fig. 10*C*, *right panel*, the $CCR5^+CCR2^+$ cells were, in fact, the best responders to conditioned medium from LPS-treated human monocyte-derived macrophages. The relationships among the cell subsets in functional responses and other features are summarized diagrammatically in Fig. 11.

Discussion

Given that T cells act primarily through short-distance interactions in lymphoid organs and peripheral tissues, the expression of shared homing receptors serves as an organizing principle for identifying T cell subsets of common function. We analyzed human effector/memory $CD4^+$ T cells based on their expression of CCR5 and CCR2. Our data suggest a pathway of progressive differentiation from $CCR5^-CCR2^-$ to $CCR5^+CCR2^-$ to $CCR5^+CCR2^+$ cells. The plausibility of this pathway is supported by the pattern of expression of surface markers, such as CD62L, CD122, and CD132, by TREC numbers, reflecting a history of increasing numbers of cell divisions, and by a series of functional assays demonstrating an increasing gradient of memory character, as depicted in Fig. 11. Our data on the $CCR5^-CCR2^-$, $CCR5^+CCR2^-$, and $CCR5^+CCR2^+$ cells separated further based on expression of CCR7 suggest that the association of CCR5 and CCR2 with differentiation is independent of CCR7, the signature marker whose presence or absence has been used to define the T_{CM} and T_{EM} populations, respectively.

The simultaneous analysis of multiple inflammatory chemokine receptors on effector/memory cells suggested that patterns of receptor coexpression might reflect a hierarchy of probabilities of induction during T cell activation. Based on our data, conditions for induction of CCR4 would be relatively relaxed and encountered frequently, whereas those for induction of CCR2 would be more stringent and satisfied infrequently. Cells would tend to accumulate additional receptors with increasing duration and/or numbers of activations and/or cell divisions, and receptor expression would be maintained when cells came to rest.

From analyzing cells ex vivo it is impossible, of course, to establish the in vivo precursor–product relationships. We have activated and cultured purified $CCR5^-CCR2^-$, $CCR5^+CCR2^-$, and $CCR5^+CCR2^+$ cells under Th1, Th2, Th17, and nonpolarizing in vitro, and have also "rested" cells for longer than a month in an attempt to demonstrate that the more differentiated cells can be derived from the less differentiated subsets. Whereas CCR5 could be readily upregulated on the $CCR5^-CCR2^-$ cells, we were not able to induce, or in fact maintain, the expression of CCR2 in vitro (data not shown). Although these results are consistent with our hypothesis that requirements for CCR2 expression are stringent, to date these experiments have not been helpful in establishing the precursors and pathways for generating the $CCR5^+CCR2^+$ cells. CCR2 expression may require a prolonged period of quiescence that is difficult to achieve in vitro.

On the basis of their expression of multiple other chemokine receptors, cells within the $CCR5^+CCR2^+$ subset would be anticipated to respond to as many as 15 different chemokines, many of which would be induced simultaneously by inflammatory stimuli. We demonstrated that cells within the $CCR5^+CCR2^+$ subset could migrate to ligands for each of five inflammation-associated receptors

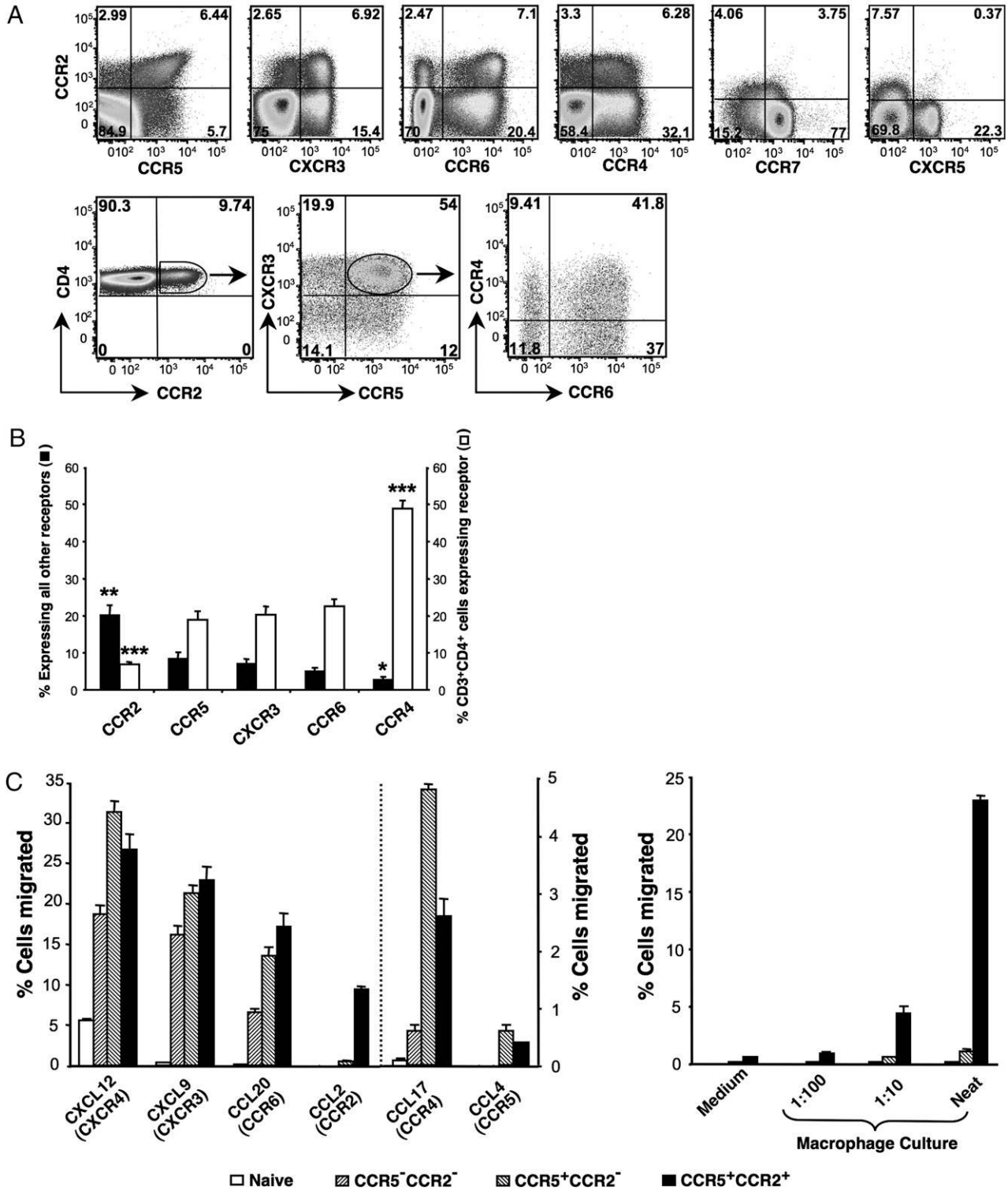

FIGURE 10. CCR2$^+$ cells express multiple species of functional chemokine receptors. *A*, PBMCs were stained with anti–CD3-Qdot605, anti–CD4-Cascade blue and anti–CCR2-biotin plus streptavidin-Qdot655, anti–CCR5-PE-Cy5, anti–CXCR3-FITC, anti–CCR6-PE, and anti–CCR4-allophycocyanin or anti–CD3-Qdot605, anti–CD4-Cascade blue, anti–CCR2-biotin plus streptavidin-PE, anti–CCR5-PE-Cy5, and anti–CCR7- or anti–CXCR5-FITC. Only CD3$^+$CD4$^+$ cells are shown. The top row shows expression of CCR2 versus other chemokine receptors individually. In the *bottom row*, sequential gating shows CCR2$^+$ cells that coexpress multiple chemokine receptors. Quadrant boundaries for each chemokine receptor were set based on samples stained with all Abs except one. Results in the *top row* for CCR5, CXCR3, CCR6, and CCR4 are from 1 donor, representative of 10, and for CCR7 and CXCR5 from 1 donor, representative of 3. *B*, For CD3$^+$CD4$^+$ cells, the open bars show percentages of cells expressing an individual chemokine receptor. For cells expressing each of those chemokine receptors, the filled bars show the percentages of cells coexpressing the other four receptors. Bars show means and SEM of results from 10 donors. $*p < 0.05$; $**p < 0.01$; and $***p < 0.001$, in comparisons with all other bars of the same type (open or filled), using two-tailed Student *t* tests. *C*, Purified CD4$^+$ T cells were sorted into naive (CD45RO$^-$) and the three CD45RO$^+$ subsets based on CCR5 and CCR2 and used in Transwell chemotaxis assays. Values are percentages of input cells that migrated to the lower wells. Bars show averages ± SEM from duplicate wells, and patterns correspond to cell subsets as shown. In the *left panel*, the *x*-axis shows the chemokines placed in the lower wells, and in parentheses the receptor for which that chemokine is a specific ligand. All chemokines were used at 1 μg/ml except for CXCL12, which was used at 100 ng/ml. The *left-hand axis*

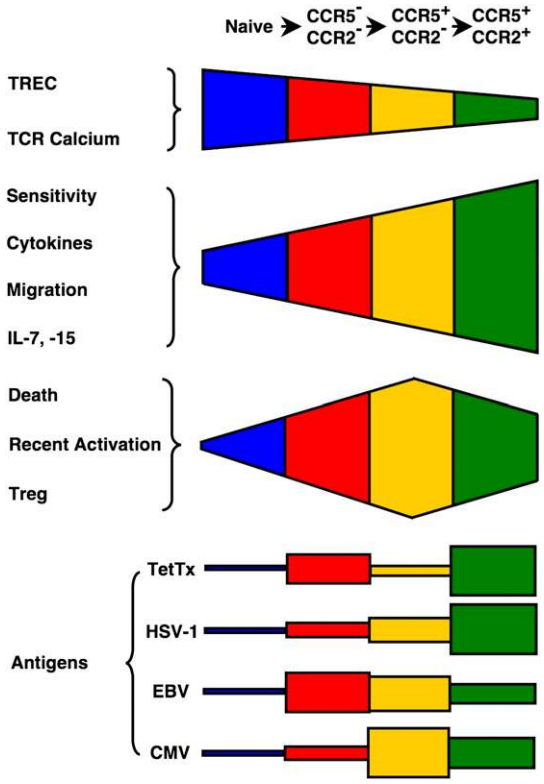

FIGURE 11. $CCR5^{-}CCR2^{-}$, $CCR5^{+}CCR2^{-}$, and $CCR5^{+}CCR2^{+}$ effector/memory subsets differ in their histories and functional responses. Relative magnitudes of the indicated parameters within the cell subsets are represented by the areas of the color-coded quadrilaterals as follows: TREC, numbers of TREC; TCR Calcium, rise in intracellular calcium following TCR ligation; Sensitivity, sensitivity to TCR-induced activation and proliferation; Cytokines, frequencies of cells producing, and rapidity of TCR-induced secretion of effector cytokines; Migration, range of chemokines to which cells respond in chemotaxis assays; IL-7, -15, proliferation in response to IL-7 and/or IL-15 and expression of IL-7Rs and IL-15Rs; Death, sensitivity to "spontaneous," FAS-, and TCR-induced cell death; Recent Activation, frequencies of cells displaying activation markers; Treg, frequencies of $CD25^{+}$ and $FOXP3^{+}$ cells; Antigens, numbers of divided cells after culturing with tetanus toxoid (TetTx) or extracts of herpesvirus-infected cells.

and responded well to products of activated macrophages. Consistent with earlier reports, we also found that $CCR2^{+}$ $CD4^{+}$ T cells express high levels of CD26 (47, 48). It is of interest not only that $CD26^{bright}$ cells could be recruited by CCL2/MCP-1 across endothelium (47, 48) but also that $CD4^{+}$ T cells capable of "spontaneous" transendothelial migration were found to be $CD26^{bright}$ (65).

Among the progressive changes in phenotypes, the $CCR5^{-}$ $CCR2^{-}$, $CCR5^{+}CCR2^{-}$, and $CCR5^{+}CCR2^{+}$ subsets showed increasing sensitivity to and rapidity of TCR-mediated activation and increasing capability to produce effector cytokines. The combined effect resulted in large differences in cytokine secretion after submaximal stimulation of the TCR. The cytokine profile of the $CCR5^{+}$ $CCR2^{+}$ subset is diverse, including cells able to produce cytokines of all the principal effector lineages. At the same time, the $CCR5^{+}$ $CCR2^{+}$ subset is relatively poor in Tregs. Together, our data suggest that the $CCR5^{+}CCR2^{+}$ subset contains cells poised to produce a rapid, broad, and potent effector response and able to migrate to any of multiple inflammation-induced chemokines, integrating functions that should equip cells to serve as the first responders to a secondary challenge.

To analyze the distribution of Ag-reactive cells within the $CCR5^{-}$ $CCR2^{-}$, $CCR5^{+}CCR2^{-}$, and $CCR5^{+}CCR2^{+}$ subsets, we evaluated proliferation to tetanus toxoid and three herpesviruses. For tetanus toxoid, the highest percentage of responding cells was in the $CCR5^{+}$ $CCR2^{+}$ subset. The relative levels of response of the $CCR5^{-}$ $CCR2^{-}$ and $CCR5^{+}CCR2^{-}$ subsets were significantly increased by removing the $CD25^{+}$ and/or $CD127^{-}$ cells. $CD127^{-}$ cells contain both Tregs and recently activated cells, as well as a small percentage of Tr-1–like cells (30, 55–58). Given the exposure history of most healthy donors to tetanus toxoid, we presume that reactivity among the subsets was representative of a "true" memory response against a long absent Ag. The poor response to tetanus toxoid that we found in the $CD127^{-}$, i.e., recently activated cells, even after partial depletion of Tregs from the $CD127^{-}$ cells by removing the $CD25^{+}$ cells, was consistent with this presumption. We conclude that the $CCR5^{+}CCR2^{+}$ subset is highly enriched in Ag-specific memory cells resulting from prior vaccination.

Herpesviruses establish life-long latency, with the potential for reactivation, and differ among themselves in a variety of ways, including their tissue tropisms. The pattern of response to HSV-1 was the most similar to that for tetanus toxoid. By contrast, for reactions to EBV, the pattern was the most "left shifted," with prominent responses in the $CCR5^{-}CCR2^{-}$ subset, which is consistent with published data for both $CD8^{+}$ and $CD4^{+}$ T cells, showing that anti-EBV cells are less differentiated than anti-CMV cells (9, 45, 66). For CMV, the response was uniformly highest in the $CCR5^{+}CCR2^{-}$ subset. For each virus, removing the $CD25^{+}$ and $CD127^{-}$ cells boosted the response within the $CCR5^{+}CCR2^{-}$ subset. Not surprisingly, the increases seen after removing the $CD25^{+}$ and $CD127^{-}$ cells were inversely related to the magnitudes of the responses found against each of the agents within the $CD25^{-}CD127^{-}$ cells themselves, which showed the rank order CMV > EBV > HSV-1 > tetanus toxoid.

Loss of CD127 and/or increased expression of CCR5 in human $CD4^{+}$ T cells have been shown in other studies immediately after immunizations with tetanus toxoid (67) or vaccinia virus (68) or during acute infection with EBV or HIV-1 (69–71). Our finding that, among the agents tested, CMV elicited the greatest responses in the $CD127^{-}$ cells, which are relatively abundant in the $CCR5^{+}$ $CCR2^{-}$ subset, is consistent with previous data (58), and suggested that CMV was the virus most often (re)stimulating a systemic immune response. These results are also consistent with data that a large percentage of memory T cells are CMV specific in infected individuals (72–74), significantly higher than for other herpesviruses (73, 75). When taken together, the Ag-specific responses suggest that the ratio of Ag-reactive cells in the $CCR5^{+}CCR2^{+}$ versus $CCR5^{+}CCR2^{-}$ subsets reflected the ratio of cells reacting to a given agent that were resting memory versus recently (re) activated—highest for tetanus toxoid and lowest for CMV.

The enrichment of the $CCR5^{+}CCR2^{-}$ subset with activated cells raised the issue of the effects of activated cells on a number of assays, particularly as they relate to our hypothetical pathway of progressive differentiation. We addressed this with experiments in which recently activated cells were removed on the basis of being $CD25^{+}$ and/or $CD127^{-}$. Although we cannot be sure that all

applies to results with CXCL12, CXCL9, CCL20, and CCL2 and the *right-hand axis* to CCL17 and CCL4. Results are from one donor, representative of four. In the *right panel*, lower wells contained medium alone, or dilutions of conditioned medium from LPS-treated macrophages. Results are from one donor, representative of three.

recently activated cells were removed in this way, the CD127$^-$ cells included almost all the cells that were HLA-DR$^+$ and/or Ki67$^+$, and downregulation of CD127 after TCR activation of human T cells is profound (57, 58). These experiments showed that the presence or absence of the activated cells did not affect our findings of an increasing sensitivity to TCR cross-linking and an increase in frequencies of effector cytokine-capable cells from the CCR5$^-$CCR2$^-$ to CCR5$^+$CCR2$^-$ to CCR5$^+$CCR2$^+$ subsets. In addition, when limiting our analysis to the CD127$^+$ cells, we found a gradient in CD127 expression that followed the same pattern (see below). Together these data suggest that the findings that underlie our ordering of the CCR5$^-$CCR2$^-$, CCR5$^+$CCR2$^-$, and CCR5$^+$CCR2$^+$ subsets along a pathway of differentiation are, in fact, features of the resting memory population. Nonetheless, the activated and/or regulatory cells clearly affected other aspects of our results, such as the Ag-specific responses and susceptibility to apoptosis.

Regulatory and/or activated cells, which are hypersensitive to death-inducing signals (58, 62, 63), contributed to the increased susceptibility to Fas-mediated death in the CCR5$^+$CCR2$^-$ subset. Enhanced death within the CCR5$^+$CCR2$^-$ subset may be related to the need to limit T cell-mediated pathology from chronically or repeatedly activated cells, such as those responding to CMV. Given that increasing T cell differentiation has also been associated with increasing sensitivity to apoptosis (33–35), it was notable that the more differentiated CCR5$^+$CCR2$^+$ cells were in fact less susceptible to death than the CCR5$^+$CCR2$^-$ cells. The relative resistance of the CCR5$^+$CCR2$^+$ cells to death was associated with high levels of BCL-2 and cFLIP, antiapoptotic proteins within the intrinsic (cytokine withdrawal) and extrinsic (Fas- or TCR-mediated) pathways, respectively. It is of interest that CCL2/MCP-1 has been reported to protect activated mouse CD8$^+$ T cells from death due to cytokine withdrawal (76) and to be important for survival of CD8$^+$ T_{EM} in mice (77). However, in our assays of spontaneous and FAS-mediated death, we saw no protective effect of adding CCL2/MCP-1 (data not shown).

IL-7 is the most important factor for homeostatic proliferation and survival of memory CD4$^+$ T cells, with IL-15 also playing a role (78). We found a gradient from the CCR5$^-$CCR2$^-$ to CCR5$^+$CCR2$^-$ to CCR5$^+$CCR2$^+$ cells in responsiveness to IL-7 and/or IL-15, and consistent with this pattern of response, we found a coincident increase among the subsets in surface staining for CD122 and CD132. For CD127, the high levels in the CCR5$^+$ CCR2$^+$ subset may be an important contributor to the BCL-2 levels in these cells, because IL-7 functions as a survival factor in part through the induction of BCL-2 family members (64).

Our data suggest that highly differentiated effector/memory populations are not necessarily unstable. Stability within the T_{EM}-like CD4$^+$ populations that are derived from differentiated effector cells is also supported by recent findings in mice (30, 31) and provides a mechanism whereby the full repertoire of cells generated during the initial, and presumably protective, response can be maintained. Our findings suggest that earlier data that T_{EM}-like cells are inherently short lived may have reflected the enrichment of T_{EM}-phenotype cells with populations that were recently and/or chronically activated. Moreover, our data showing Ag/agent-dependent differences in the magnitudes of responses in CD25$^-$ CD127$^-$ versus CD25$^-$CD127$^+$ cells suggest that activated cells may constitute a separate Ag-driven population that does not consist principally of memory cells undergoing homeostatic turnover.

Experiments in infection models in mice have shown the importance of effector function and migration into tissue in host defense against an acute infection (79) and have demonstrated the role of T_{EM}-like cells in mediating protection early during a recall response (28, 80). The CCR5$^+$CCR2$^+$ cells would seem good candidates to function in such a role in humans, and our data suggest that these cells, once produced through vaccination or infection, could contribute to Ag-specific long-lived memory.

Acknowledgments

We thank Calman Prussin, Satya Singh, and Jeffrey Cohen, National Institute of Allergy and Infectious Diseases, for helpful discussions and/or for critical reading of the manuscript; Jagan Muppidi, National Institute of Arthritis and Musculoskeletal and Skin Diseases, for advice on cell death assays; Irini Sereti, National Institute of Allergy and Infectious Diseases, for consultation and assistance; and members of the Flow Cytometry Section, Research Technologies Branch, National Institute of Allergy and Infectious Diseases, including Kevin Holmes, Calvin Eigsti, Bishop Hague, David Stephany, and Elina Stregevsky, for consultation and expert technical assistance.

Disclosures

The authors have no financial conflicts of interest.

References

1. Seder, R. A., P. A. Darrah, and M. Roederer. 2008. T-cell quality in memory and protection: implications for vaccine design. *Nat. Rev. Immunol.* 8: 247–258.
2. van den Brink, M. R., O. Alpdogan, and R. L. Boyd. 2004. Strategies to enhance T-cell reconstitution in immunocompromised patients. *Nat. Rev. Immunol.* 4: 856–867.
3. Parish, I. A., and S. M. Kaech. 2009. Diversity in CD8(+) T cell differentiation. *Curr. Opin. Immunol.* 21: 291–297.
4. Murphy, K. M., and S. L. Reiner. 2002. The lineage decisions of helper T cells. *Nat. Rev. Immunol.* 2: 933–944.
5. MacLeod, M. K., E. T. Clambey, J. W. Kappler, and P. Marrack. 2009. CD4 memory T cells: what are they and what can they do? *Semin. Immunol.* 21: 53–61.
6. Battaglia, M., S. Gregori, R. Bacchetta, and M. G. Roncarolo. 2006. Tr1 cells: from discovery to their clinical application. *Semin. Immunol.* 18: 120–127.
7. Harrington, L. E., R. D. Hatton, P. R. Mangan, H. Turner, T. L. Murphy, K. M. Murphy, and C. T. Weaver. 2005. Interleukin 17-producing CD4+ effector T cells develop via a lineage distinct from the T helper type 1 and 2 lineages. *Nat. Immunol.* 6: 1123–1132.
8. Sakaguchi, S. 2004. Naturally arising CD4+ regulatory t cells for immunologic self-tolerance and negative control of immune responses. *Annu. Rev. Immunol.* 22: 531–562.
9. Amyes, E., C. Hatton, D. Montamat-Sicotte, N. Gudgeon, A. B. Rickinson, A. J. McMichael, and M. F. Callan. 2003. Characterization of the CD4+ T cell response to Epstein-Barr virus during primary and persistent infection. *J. Exp. Med.* 198: 903–911.
10. Ohara, T., K. Koyama, Y. Kusunoki, T. Hayashi, N. Tsuyama, Y. Kubo, and S. Kyoizumi. 2002. Memory functions and death proneness in three CD4+ CD45RO+ human T cell subsets. *J. Immunol.* 169: 39–48.
11. Garside, P., E. Ingulli, R. R. Merica, J. G. Johnson, R. J. Noelle, and M. K. Jenkins. 1998. Visualization of specific B and T lymphocyte interactions in the lymph node. *Science* 281: 96–99.
12. Dutton, R. W., L. M. Bradley, and S. L. Swain. 1998. T cell memory. *Annu. Rev. Immunol.* 16: 201–223.
13. Springer, T. A. 1994. Traffic signals for lymphocyte recirculation and leukocyte emigration: the multistep paradigm. *Cell* 76: 301–314.
14. Arbonés, M. L., D. C. Ord, K. Ley, H. Ratech, C. Maynard-Curry, G. Otten, D. J. Capon, and T. F. Tedder. 1994. Lymphocyte homing and leukocyte rolling and migration are impaired in L-selectin-deficient mice. *Immunity* 1: 247–260.
15. Förster, R., A. Schubel, D. Breitfeld, E. Kremmer, I. Renner-Müller, E. Wolf, and M. Lipp. 1999. CCR7 coordinates the primary immune response by establishing functional microenvironments in secondary lymphoid organs. *Cell* 99: 23–33.
16. Sallusto, F., D. Lenig, R. Förster, M. Lipp, and A. Lanzavecchia. 1999. Two subsets of memory T lymphocytes with distinct homing potentials and effector functions. *Nature* 401: 708–712.
17. Sallusto, F., J. Geginat, and A. Lanzavecchia. 2004. Central memory and effector memory T cell subsets: function, generation, and maintenance. *Annu. Rev. Immunol.* 22: 745–763.
18. Lanzavecchia, A., and F. Sallusto. 2005. Understanding the generation and function of memory T cell subsets. *Curr. Opin. Immunol.* 17: 326–332.
19. Harris, N. L., V. Watt, F. Ronchese, and G. Le Gros. 2002. Differential T cell function and fate in lymph node and nonlymphoid tissues. *J. Exp. Med.* 195: 317–326.
20. Reinhardt, R. L., A. Khoruts, R. Merica, T. Zell, and M. K. Jenkins. 2001. Visualizing the generation of memory CD4 T cells in the whole body. *Nature* 410: 101–105.

21. Masopust, D., V. Vezys, A. L. Marzo, and L. Lefrançois. 2001. Preferential localization of effector memory cells in nonlymphoid tissue. *Science* 291: 2413–2417.
22. Román, E., E. Miller, A. Harmsen, J. Wiley, U. H. Von Andrian, G. Huston, and S. L. Swain. 2002. CD4 effector T cell subsets in the response to influenza: heterogeneity, migration, and function. *J. Exp. Med.* 196: 957–968.
23. Wherry, E. J., V. Teichgräber, T. C. Becker, D. Masopust, S. M. Kaech, R. Antia, U. H. von Andrian, and R. Ahmed. 2003. Lineage relationship and protective immunity of memory CD8 T cell subsets. *Nat. Immunol.* 4: 225–234.
24. Marzo, A. L., K. D. Klonowski, A. Le Bon, P. Borrow, D. F. Tough, and L. Lefrançois. 2005. Initial T cell frequency dictates memory CD8+ T cell lineage commitment. *Nat. Immunol.* 6: 793–799.
25. Wu, C. Y., J. R. Kirman, M. J. Rotte, D. F. Davey, S. P. Perfetto, E. G. Rhee, B. L. Freidag, B. J. Hill, D. C. Douek, and R. A. Seder. 2002. Distinct lineages of T(H)1 cells have differential capacities for memory cell generation in vivo. *Nat. Immunol.* 3: 852–858.
26. Moulton, V. R., N. D. Bushar, D. B. Leeser, D. S. Patke, and D. L. Farber. 2006. Divergent generation of heterogeneous memory CD4 T cells. *J. Immunol.* 177: 869–876.
27. Zaph, C., J. Uzonna, S. M. Beverley, and P. Scott. 2004. Central memory T cells mediate long-term immunity to *Leishmania major* in the absence of persistent parasites. *Nat. Med.* 10: 1104–1110.
28. Roberts, A. D., and D. L. Woodland. 2004. Cutting edge: effector memory CD8+ T cells play a prominent role in recall responses to secondary viral infection in the lung. *J. Immunol.* 172: 6533–6537.
29. Bingaman, A. W., D. S. Patke, V. R. Mane, M. Ahmadzadeh, M. Ndejembi, S. T. Bartlett, and D. L. Farber. 2005. Novel phenotypes and migratory properties distinguish memory CD4 T cell subsets in lymphoid and lung tissue. *Eur. J. Immunol.* 35: 3173–3186.
30. Löhning, M., A. N. Hegazy, D. D. Pinschewer, D. Busse, K. S. Lang, T. Höfer, A. Radbruch, R. M. Zinkernagel, and H. Hengartner. 2008. Long-lived virus-reactive memory T cells generated from purified cytokine-secreting T helper type 1 and type 2 effectors. *J. Exp. Med.* 205: 53–61.
31. Harrington, L. E., K. M. Janowski, J. R. Oliver, A. J. Zajac, and C. T. Weaver. 2008. Memory CD4 T cells emerge from effector T-cell progenitors. *Nature* 452: 356–360.
32. Macallan, D. C., D. Wallace, Y. Zhang, C. De Lara, A. T. Worth, H. Ghattas, G. E. Griffin, P. C. Beverley, and D. F. Tough. 2004. Rapid turnover of effector-memory CD4(+) T cells in healthy humans. *J. Exp. Med.* 200: 255–260.
33. Rivino, L., M. Messi, D. Jarrossay, A. Lanzavecchia, F. Sallusto, and J. Geginat. 2004. Chemokine receptor expression identifies Pre-T helper (Th)1, Pre-Th2, and nonpolarized cells among human CD4+ central memory T cells. *J. Exp. Med.* 200: 725–735.
34. Fritsch, R. D., X. Shen, G. P. Sims, K. S. Hathcock, R. J. Hodes, and P. E. Lipsky. 2005. Stepwise differentiation of CD4 memory T cells defined by expression of CCR7 and CD27. *J. Immunol.* 175: 6489–6497.
35. Riou, C., B. Yassine-Diab, J. Van grevenynghe, R. Somogyi, L. D. Greller, D. Gagnon, S. Gimmig, P. Wilkinson, Y. Shi, M. J. Cameron, et al. 2007. Convergence of TCR and cytokine signaling leads to FOXO3a phosphorylation and drives the survival of CD4+ central memory T cells. *J. Exp. Med.* 204: 79–91.
36. Blanpain, C., F. Libert, G. Vassart, and M. Parmentier. 2002. CCR5 and HIV infection. *Receptors Channels* 8: 19–31.
37. Charo, I. F., and W. Peters. 2003. Chemokine receptor 2 (CCR2) in atherosclerosis, infectious diseases, and regulation of T-cell polarization. *Microcirculation* 10: 259–264.
38. Kim, C. H., L. Rott, E. J. Kunkel, M. C. Genovese, D. P. Andrew, L. Wu, and E. C. Butcher. 2001. Rules of chemokine receptor association with T cell polarization in vivo. *J. Clin. Invest.* 108: 1331–1339.
39. Doranz, B. J., J. Rucker, Y. J. Yi, R. J. Smyth, M. Samson, S. C. Peiper, M. Parmentier, R. G. Collman, and R. W. Doms. 1996. A dual-tropic primary HIV-1 isolate that uses fusin and the beta-chemokine receptors CKR-5, CKR-3, and CKR-2b as fusion cofactors. *Cell* 85: 1149–1158.
40. Douek, D. C., R. D. McFarland, P. H. Keiser, E. A. Gage, J. M. Massey, B. F. Haynes, M. A. Polis, A. T. Haase, M. B. Feinberg, J. L. Sullivan, et al. 1998. Changes in thymic function with age and during the treatment of HIV infection. *Nature* 396: 690–695.
41. De Rosa, S. C., L. A. Herzenberg, L. A. Herzenberg, and M. Roederer. 2001. 11-color, 13-parameter flow cytometry: identification of human naive T cells by phenotype, function, and T-cell receptor diversity. *Nat. Med.* 7: 245–248.
42. Picker, L. J., J. R. Treer, B. Ferguson-Darnell, P. A. Collins, D. Buck, and L. W. Terstappen. 1993. Control of lymphocyte recirculation in man. I. Differential regulation of the peripheral lymph node homing receptor L-selectin on T cells during the virgin to memory cell transition. *J. Immunol.* 150: 1105–1121.
43. Hengel, R. L., V. Thaker, M. V. Pavlick, J. A. Metcalf, G. Dennis, Jr., J. Yang, R. A. Lempicki, I. Sereti, and H. C. Lane. 2003. Cutting edge: L-selectin (CD62L) expression distinguishes small resting memory CD4+ T cells that preferentially respond to recall antigen. *J. Immunol.* 170: 28–32.
44. Song, K., R. L. Rabin, B. J. Hill, S. C. De Rosa, S. P. Perfetto, H. H. Zhang, J. F. Foley, J. S. Reiner, J. Liu, J. J. Mattapallil, et al. 2005. Characterization of subsets of CD4+ memory T cells reveals early branched pathways of T cell differentiation in humans. *Proc. Natl. Acad. Sci. USA* 102: 7916–7921.
45. Appay, V., P. R. Dunbar, M. Callan, P. Klenerman, G. M. Gillespie, L. Papagno, G. S. Ogg, A. King, F. Lechner, C. A. Spina, et al. 2002. Memory CD8+ T cells vary in differentiation phenotype in different persistent virus infections. *Nat. Med.* 8: 379–385.
46. Yue, F. Y., C. M. Kovacs, R. C. Dimayuga, P. Parks, and M. A. Ostrowski. 2004. HIV-1-specific memory CD4+ T cells are phenotypically less mature than cytomegalovirus-specific memory CD4+ T cells. *J. Immunol.* 172: 2476–2486.
47. Carr, M. W., S. J. Roth, E. Luther, S. S. Rose, and T. A. Springer. 1994. Monocyte chemoattractant protein 1 acts as a T-lymphocyte chemoattractant. *Proc. Natl. Acad. Sci. USA* 91: 3652–3656.
48. Qin, S., G. LaRosa, J. J. Campbell, H. Smith-Heath, N. Kassam, X. Shi, L. Zeng, E. C. Buthcher, and C. R. Mackay. 1996. Expression of monocyte chemoattractant protein-1 and interleukin-8 receptors on subsets of T cells: correlation with transendothelial chemotactic potential. *Eur. J. Immunol.* 26: 640–647.
49. Bingaman, A. W., and D. L. Farber. 2004. Memory T cells in transplantation: generation, function, and potential role in rejection. *Am. J. Transplant.* 4: 846–852.
50. Farber, D. L. 2009. Biochemical signaling pathways for memory T cell recall. *Semin. Immunol.* 21: 84–91.
51. Roederer, M., M. Bigos, T. Nozaki, R. T. Stovel, D. R. Parks, and L. A. Herzenberg. 1995. Heterogeneous calcium flux in peripheral T cell subsets revealed by five-color flow cytometry using log-ratio circuitry. *Cytometry* 21: 187–196.
52. Hall, S. R., B. M. Heffernan, N. T. Thompson, and W. C. Rowan. 1999. CD4+ CD45RA+ and CD4+ CD45RO+ T cells differ in their TCR-associated signaling responses. *Eur. J. Immunol.* 29: 2098–2106.
53. Clark, A. 2000. Post-transcriptional regulation of pro-inflammatory gene expression. *Arthritis Res.* 2: 172–174.
54. Park, J. H., Q. Yu, B. Erman, J. S. Appelbaum, D. Montoya-Durango, H. L. Grimes, and A. Singer. 2004. Suppression of IL7Ralpha transcription by IL-7 and other prosurvival cytokines: a novel mechanism for maximizing IL-7-dependent T cell survival. *Immunity* 21: 289–302.
55. Liu, W., A. L. Putnam, Z. Xu-Yu, G. L. Szot, M. R. Lee, S. Zhu, P. A. Gottlieb, P. Kapranov, T. R. Gingeras, B. Fazekas de St Groth, et al. 2006. CD127 expression inversely correlates with FoxP3 and suppressive function of human CD4+ T reg cells. *J. Exp. Med.* 203: 1701–1711.
56. Seddiki, N., B. Santner-Nanan, J. Martinson, J. Zaunders, S. Sasson, A. Landay, M. Solomon, W. Selby, S. I. Alexander, R. Nanan, et al. 2006. Expression of interleukin (IL)-2 and IL-7 receptors discriminates between human regulatory and activated T cells. *J. Exp. Med.* 203: 1693–1700.
57. Alves, N. L., E. M. van Leeuwen, I. A. Derks, and R. A. van Lier. 2008. Differential regulation of human IL-7 receptor alpha expression by IL-7 and TCR signaling. *J. Immunol.* 180: 5201–5210.
58. Häringer, B., L. Lozza, B. Steckel, and J. Geginat. 2009. Identification and characterization of IL-10/IFN-gamma-producing effector-like T cells with regulatory function in human blood. *J. Exp. Med.* 206: 1009–1017.
59. Wang, J., A. Ioan-Facsinay, E. I. van der Voort, T. W. Huizinga, and R. E. Toes. 2007. Transient expression of FOXP3 in human activated nonregulatory CD4+ T cells. *Eur. J. Immunol.* 37: 129–138.
60. Yagi, H., T. Nomura, K. Nakamura, S. Yamazaki, T. Kitawaki, S. Hori, M. Maeda, M. Onodera, T. Uchiyama, S. Fujii, and S. Sakaguchi. 2004. Crucial role of FOXP3 in the development and function of human CD25+CD4+ regulatory T cells. *Int. Immunol.* 16: 1643–1656.
61. Roncador, G., P. J. Brown, L. Maestre, S. Hue, J. L. Martínez-Torrecuadrada, K. L. Ling, S. Pratap, C. Toms, B. C. Fox, V. Cerundolo, et al. 2005. Analysis of FOXP3 protein expression in human CD4+CD25+ regulatory T cells at the single-cell level. *Eur. J. Immunol.* 35: 1681–1691.
62. Fritzsching, B., N. Oberle, N. Eberhardt, S. Quick, J. Haas, B. Wildemann, P. H. Krammer, and E. Suri-Payer. 2005. In contrast to effector T cells, CD4+CD25+FoxP3+ regulatory T cells are highly susceptible to CD95 ligand- but not to TCR-mediated cell death. *J. Immunol.* 175: 32–36.
63. Krammer, P. H., R. Arnold, and I. N. Lavrik. 2007. Life and death in peripheral T cells. *Nat. Rev. Immunol.* 7: 532–542.
64. Jiang, Q., W. Q. Li, F. B. Aiello, R. Mazzucchelli, B. Asefa, A. R. Khaled, and S. K. Durum. 2005. Cell biology of IL-7, a key lymphotrophin. *Cytokine Growth Factor Rev.* 16: 513–533.
65. Brezinschek, R. I., P. E. Lipsky, P. Galea, R. Vita, and N. Oppenheimer-Marks. 1995. Phenotypic characterization of CD4+ T cells that exhibit a transendothelial migratory capacity. *J. Immunol.* 154: 3062–3077.
66. Heller, K. N., J. Upshaw, B. Seyoum, H. Zebroski, and C. Münz. 2007. Distinct memory CD4+ T-cell subsets mediate immune recognition of Epstein Barr virus nuclear antigen 1 in healthy virus carriers. *Blood* 109: 1138–1146.
67. Cellerai, C., A. Harari, F. Vallelian, O. Boyman, and G. Pantaleo. 2007. Functional and phenotypic characterization of tetanus toxoid-specific human CD4+ T cells following re-immunization. *Eur. J. Immunol.* 37: 1129–1138.
68. Zaunders, J. J., W. B. Dyer, M. L. Munier, S. Ip, J. Liu, E. Amyes, W. Rawlinson, R. De Rose, S. J. Kent, J. S. Sullivan, et al. 2006. CD127+CCR5+CD38+++ CD4+ Th1 effector cells are an early component of the primary immune response to vaccinia virus and precede development of interleukin-2+ memory CD4+ T cells. *J. Virol.* 80: 10151–10161.
69. Zaunders, J. J., G. R. Kaufmann, P. H. Cunningham, D. Smith, P. Grey, K. Suzuki, A. Carr, L. E. Goh, and D. A. Cooper. 2001. Increased turnover of CCR5+ and redistribution of CCR5- CD4 T lymphocytes during primary human immunodeficiency virus type 1 infection. *J. Infect. Dis.* 183: 736–743.
70. Zaunders, J. J., L. Moutouh-de Parseval, S. Kitada, J. C. Reed, S. Rought, D. Genini, L. Leoni, A. Kelleher, D. A. Cooper, D. E. Smith, et al. 2003. Polyclonal proliferation and apoptosis of CCR5+ T lymphocytes during primary human immunodeficiency virus type 1 infection: regulation by interleukin (IL)-2, IL-15, and Bcl-2. *J. Infect. Dis.* 187: 1735–1747.
71. Zaunders, J. J., M. L. Munier, D. E. Kaufmann, S. Ip, P. Grey, D. Smith, T. Ramacciotti, D. Quan, R. Finlayson, J. Kaldor, et al. 2005. Early proliferation

of CCR5(+) CD38(+++) antigen-specific CD4(+) Th1 effector cells during primary HIV-1 infection. *Blood* 106: 1660–1667.
72. Asanuma, H., M. Sharp, H. T. Maecker, V. C. Maino, and A. M. Arvin. 2000. Frequencies of memory T cells specific for varicella-zoster virus, herpes simplex virus, and cytomegalovirus by intracellular detection of cytokine expression. *J. Infect. Dis.* 181: 859–866.
73. Fletcher, J. M., M. Vukmanovic-Stejic, P. J. Dunne, K. E. Birch, J. E. Cook, S. E. Jackson, M. Salmon, M. H. Rustin, and A. N. Akbar. 2005. Cytomegalovirus-specific CD4+ T cells in healthy carriers are continuously driven to replicative exhaustion. *J. Immunol.* 175: 8218–8225.
74. Sylwester, A. W., B. L. Mitchell, J. B. Edgar, C. Taormina, C. Pelte, F. Ruchti, P. R. Sleath, K. H. Grabstein, N. A. Hosken, F. Kern, et al. 2005. Broadly targeted human cytomegalovirus-specific CD4+ and CD8+ T cells dominate the memory compartments of exposed subjects. *J. Exp. Med.* 202: 673–685.
75. van Leeuwen, E. M., G. J. de Bree, E. B. Remmerswaal, S. L. Yong, K. Tesselaar, I. J. ten Berge, and R. A. van Lier. 2005. IL-7 receptor alpha chain expression distinguishes functional subsets of virus-specific human CD8+ T cells. *Blood* 106: 2091–2098.
76. Diaz-Guerra, E., R. Vernal, M. J. del Prete, A. Silva, and J. A. Garcia-Sanz. 2007. CCL2 inhibits the apoptosis program induced by growth factor deprivation, rescuing functional T cells. *J. Immunol.* 179: 7352–7357.
77. Wang, T., H. Dai, N. Wan, Y. Moore, and Z. Dai. 2008. The role for monocyte chemoattractant protein-1 in the generation and function of memory CD8+ T cells. *J. Immunol.* 180: 2886–2893.
78. Surh, C. D., and J. Sprent. 2008. Homeostasis of naive and memory T cells. *Immunity* 29: 848–862.
79. Maloy, K. J., C. Burkhart, T. M. Junt, B. Odermatt, A. Oxenius, L. Piali, R. M. Zinkernagel, and H. Hengartner. 2000. CD4(+) T cell subsets during virus infection. Protective capacity depends on effector cytokine secretion and on migratory capability. *J. Exp. Med.* 191: 2159–2170.
80. Hogan, R. J., W. Zhong, E. J. Usherwood, T. Cookenham, A. D. Roberts, and D. L. Woodland. 2001. Protection from respiratory virus infections can be mediated by antigen-specific CD4(+) T cells that persist in the lungs. *J. Exp. Med.* 193: 981–986.